JGR Atmospheres

RESEARCH ARTICLE
10.1029/2021JD035498

Key Points:

- Climatology of the vertical profiles of polarimetric radar variables and microphysical parameters is documented for different storm types
- Areas of high ice water content (IWC) in clouds are characterized by high values of specific differential phase combined with low reflectivity
- Tropical clouds have smaller size ice in higher concentration compared to their continental counterparts with comparable IWC

Supporting Information:

Supporting Information may be found in the online version of this article.

Correspondence to:

J. Hu,
jiaxi.hu@noaa.gov

Citation:

Hu, J., & Ryzhkov, A. (2022). Climatology of the vertical profiles of polarimetric radar variables and retrieved microphysical parameters in continental/tropical MCSs and landfalling hurricanes. *Journal of Geophysical Research: Atmospheres*, *127*, e2021JD035498. https://doi.org/10.1029/2021JD035498

Received 1 JUL 2021
Accepted 9 FEB 2022

Climatology of the Vertical Profiles of Polarimetric Radar Variables and Retrieved Microphysical Parameters in Continental/Tropical MCSs and Landfalling Hurricanes

Jiaxi Hu[1,2] and Alexander Ryzhkov[1,2]

[1]Cooperative Institute for Severe and High-Impact Weather Research and Operations, University of Oklahoma, Norman, OK, USA, [2]NOAA/OAR National Severe Storms Laboratory, Norman, OK, USA

Abstract Most existing cloud models tend to overestimate the size of cloud ice particles and underestimate their concentration. This emphasizes the need to provide a reliable observational reference to optimize cloud model performance, particularly in areas of high concentration of ice at high altitudes. The dual-polarization radars give the community a unique opportunity to quantify cloud ice with a good accuracy using polarimetric radar retrievals. In this study, we utilize the network of operational WSR-88D radars to build a climatology of the vertical profiles of radar variables, such as radar reflectivity Z, differential reflectivity Z_{DR}, and specific differential phase K_{DP} as well as the radar-retrieved vertical profiles of ice water content (IWC) above the melting layer and liquid water content below it, mean volume diameter D_m, and total number concentration N_t of ice and liquid particles. Such climatology was created for continental/marine mesoscale convective systems (MCSs) and tropical cyclones including hurricanes. The dataset includes 13 continental MCSs, 10 marine MCSs, and 11 tropical cyclones. Separate statistics of the "background" vertical profiles and the ones associated with high IWC aloft have been obtained in the course of this study. It is shown that continental MCSs exhibit larger size of ice in lower concentration aloft compared to the marine MCSs and especially tropical cyclones/hurricanes. A combination of high K_{DP} and low Z aloft signifies lower D_m, higher N_t, and often substantial IWC.

1. Introduction

Modern operational radar networks around the world are equipped with Doppler polarimetric radars which demonstrate their efficiency in improving data quality, quantitative precipitation estimation, hydrometeor classification, and severe weather warnings (Bringi & Chandrasekar, 2001; Kumjian, 2018; Ryzhkov & Zrnic, 2019; Zhang, 2016). In addition to the radar reflectivity Z, polarimetric radars directly measure differential reflectivity Z_{DR} which is a difference between the reflectivities at orthogonal polarizations, differential phase Φ_{DP} which is the difference between the phases of reflected signals at orthogonal polarizations, and cross-correlation coefficient ρ_{hv} between orthogonally polarized radar returns. A very important polarimetric variable, specific differential phase K_{DP}, is estimated from a radial profile of Φ_{DP} as a half of the radial derivative of Φ_{DP}. Polarimetric radar measurements can be efficiently utilized for retrievals of key microphysical variables, such as precipitation fluxes, liquid water content (LWC) or ice water content (IWC), particle characteristic sizes, and their number concentrations.

Polarimetric weather radars also offer a unique opportunity to optimize numerical weather prediction (NWP) models (Ryzhkov et al., 2020). The inability of existing microphysical parameterization schemes in the NWP models to adequately capture the complexity of various microphysical processes is commonly blamed as a main source of forecast uncertainties (e.g., Fan et al., 2017; Morrison et al., 2015, 2020). Because the polarimetric radars are capable of distinguishing between hydrometeors with different microphysical properties and identifying "polarimetric fingerprints" of various microphysical processes, they are a powerful resource for optimization of cloud models (e.g., Kennedy & Rutledge, 2011; Kumjian et al., 2013, 2014; Kumjian & Ryzhkov, 2009, 2010, 2012; Ryzhkov et al., 2013).

Reliable radar microphysical retrievals provide important references for the optimization of microphysical parameterizations in NWP models because these retrievals yield estimates of LWC/IWC, mean volume diameter D_m, and total number concentration N_t of hydrometeors over large regions of a storm. It is known that existing NWP models tend to ubiquitously overestimate the size of ice and underestimate its number concentration, particularly

in the areas of high-altitude ice in significant concentration with high IWC (HIWC; e.g., Fridlind et al., 2015; Huang et al., 2021; Stanford et al., 2017). One of the possible reasons for such persistent model biases is that the secondary ice production (SIP) may not be appropriately accounted for in the models (Korolev & Leisner, 2020).

Significant differences were documented between microphysical characteristics of maritime tropical and midlatitude continental storms. These are rooted in the differences in vertical profiles of humidity, cloud condensation nuclei (CCN) concentrations, strengths of updrafts, and possibly SIP mechanisms among other factors. A bulk of tropical rain forms primarily via a warm rain process with ice playing a relatively minor role in its production compared to the midlatitude storms where a good portion of rain is generated from melting graupel. In stronger convective updrafts typical for continental storms, most of a secondary ice is likely produced via collision-induced breakup whereas freezing drop shattering may be a dominant SIP mechanism in tropical maritime updrafts (Khain & Pinsky, 2018). It is hard to quantify ice within the convective updrafts even with polarimetric radars but it is much easier to estimate multiple ice attributes after it is advected into the stratiform part of the storm where graupel/hail is not common and where the suggested polarimetric retrievals are quite accurate. Because tropical and continental ice and rain are formed via different microphysical processes, it would be instrumental to statistically compare vertical profiles of their radar and microphysical characteristics using a unified approach based on the observations with a multitude of operational WSR-88D weather radars. This is one of the main objectives of this study.

Polarimetric radar retrievals in pure rain are pretty well established. For the rain rate estimation, a novel method based on specific attenuation A and specific differential phase K_{DP} introduced by Ryzhkov et al. (2013) proved to be quite efficient at S band as its validation using the United States National Weather Service WSR-88D radars demonstrated (Zhang et al., 2020). LWC can be effectively estimated using both the radar reflectivity Z and differential reflectivity Z_{DR} (see Ryzhkov & Zrnic, 2019; Zhang, 2016). The mean volume diameter of raindrops D_m is traditionally estimated from Z_{DR} (e.g., Brandes et al., 2004; Bringi et al., 2009; Cao et al., 2008; Zhang et al., 2001). The overviews of the polarimetric retrievals in rain can be found in Zhang (2016) and Ryzhkov and Zrnic (2019).

Radar retrievals in ice are much more difficult than in rain due to tremendous diversity of ice habits. Until recently, radar reflectivity Z was the only radar parameter used for estimating snowfall rate S, IWC, and size of the ice particles (Hogan et al., 2006; Kalina et al., 2017; Matrosov & Heymsfield, 2017; Protat et al., 2016; Tian et al., 2016). Because radar reflectivity is heavily weighted by a few largest snowflakes in the particle size spectrum, the Z-based retrievals are notoriously inaccurate for ice. It is known that the existing IWC(Z) relations generally tend to significantly underestimate IWC in areas of very high concentrations of small ice crystals at high altitudes. The underestimation of IWC presents potential icing hazard to aircrafts. Such ice with significant IWC is routinely reported in tropical cyclones, thunderstorm anvils, and stratiform parts of mesoscale convective systems (MCS) by in situ microphysical measurements onboard research aircrafts (Heymsfield et al., 2009; Leroy et al., 2017; McFarquhar & Heymsfield 1996; Rosenfeld & Woodley, 2000; Strapp et al., 2016).

First attempts to improve the radar estimates of IWC using polarimetric measurements were made in the studies of Vivekanandan et al. (1994) and Ryzhkov et al. (1998) followed by recent publications by Ryzhkov et al. (2018), Ryzhkov and Zrnic (2019), and Bukovcic et al. (2018, 2020) where some alternative polarimetric relations for determination of IWC were introduced. In addition, the polarimetric retrieval relations for the mean volume diameter of ice particles D_m and their total number concentration N_t have been suggested in Ryzhkov et al. (2018) and Ryzhkov and Zrnic (2019).

Polarimetric relations for ice contain specific differential phase K_{DP}. If the density-size inverse dependence of ice/snow particles is assumed, then K_{DP} is approximately proportional to the first moment of the particle size distribution (PSD) which is much closer to IWC (which is a second moment of PSD) than radar reflectivity Z which is proportional to the fourth moment of PSD of ice/snow. A bulk of snow mass is contained at the lower end of its size spectrum whereas Z is primarily sensitive to its upper end containing a few largest snowflakes. Because Z is determined by the fourth moment of PSD and K_{DP} by its first moment, their ratio is proportional to the cube of the mean volume diameter D_m and is independent of the total number concentration N_t. Therefore, D_m can be estimated from the cubic root of the Z/K_{DP} ratio. If the reflectivity difference $Z_{dp} = Z_h - Z_v = Z_h\left(1 - Z_{dr}^{-1}\right)$ is utilized instead of Z in the ratio with K_{DP} then the corresponding estimates become insensitive to the variability of

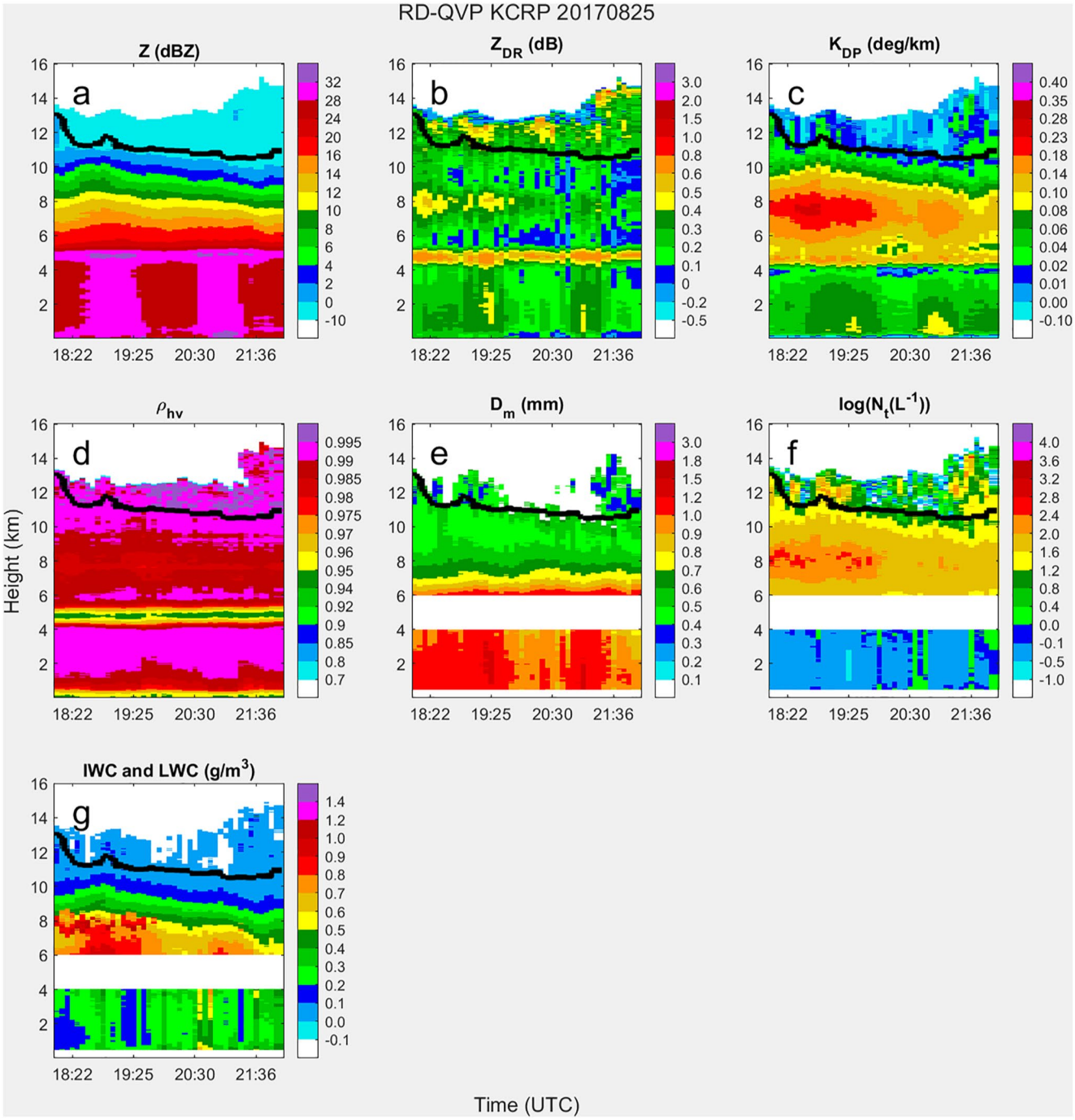

Figure 1. RD-QVP time series between 1800 UTC and 2200 UTC 25 August 2017 near Corpus Christi, Texas (KCRP), WSR-88D radar. (a) Z, (b) Z_{DR}, (c) K_{DP}, (d) ρ_{hv}, (e) D_m, (f) N_t, and (g) IWC/LWC. Black line represents the 10 dB SNR contour and pixels above this line are not used for CFAD calculations.

the particle shapes and orientations. Once D_m is calculated, the total number concentration N_t can be determined from the combination of Z and D_m.

The quality of the polarimetric retrievals of IWC has been evaluated using in situ microphysical measurements onboard research aircrafts (Kedzuf et al., 2021; Murphy et al., 2020; Nguyen et al., 2019; Ryzhkov et al., 1998) and at the surface (Bukovcic et al., 2018, 2020), whereas the corresponding retrievals of D_m and N_t have been validated by Murphy et al. (2020) and Kedzuf et al. (2021). These initial verification tests showed good promise,

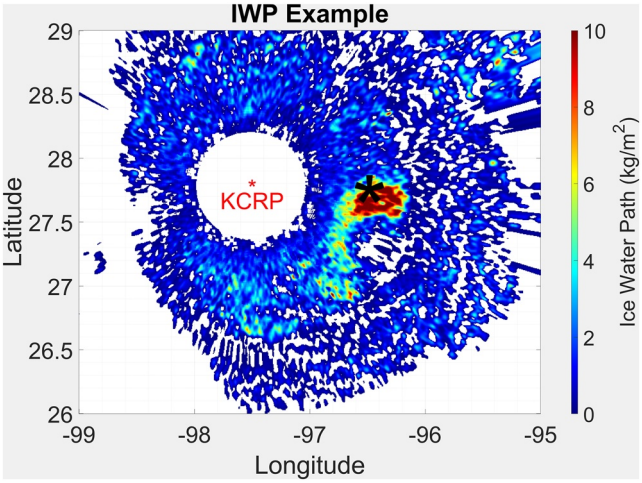

Figure 2. An example of ice water path (IWP) near Copper Christi, TX during the landfall of Hurricane Harvey on 25 August 2017 at 1812 UTC. Black asterisk denotes the center of moving HIWC area.

and the polarimetric radar retrievals in ice and rain have already been utilized in a number of recent observational studies (e.g., Homeyer et al., 2021; Hu et al., 2020; Troemel et al., 2019; Wu et al., 2021).

A cursory comparison of the vertical profiles of polarimetric variables and derived microphysical parameters in the stratiform parts of the continental MCS (Murphy et al., 2020) and tropical cyclones (Homeyer et al., 2021; Hu et al., 2020) indicates that HIWC is more typical for marine weather systems that are generally characterized by lower values of D_m and higher values of N_t in high-altitude ice. However, previous studies were either case studies or only covered a limited number of storms. The community needs to know whether the results from those studies are broadly applicable for validating numerical simulations. The operational network of polarimetric WSR-88D radars provides a unique opportunity to build a climatology of the radar and microphysical patterns in cloud and precipitation systems over the CONUS using both inland and coastal radars that are capable of observing marine MCSs and landfalling hurricanes.

Several novel methodologies for processing and visualizing radar data have been introduced recently which can help to facilitate such comprehensive statistical analysis. These methodologies include the quasi-vertical profiles (QVP; Ryzhkov et al., 2016), range-defined QVP (RD-QVP; Tobin & Kumjian, 2017), enhanced and slanted vertical profiles, respectively (Bukovcic et al., 2017), columnar vertical profiles (CVP; Murphy et al., 2020), and GridRad (Homeyer & Bowman, 2017) techniques and products.

In this study, we perform a systematic analysis of the vertical profiles of polarimetric radar variables and microphysical parameters, such as LWC/IWC, D_m, and N_t using multiple WSR-88D radars and the RD-QVP and CVP data processing techniques for various types of weather systems including continental/marine MCSs and tropical cyclones. Overall, 34 storms have been examined. The primary objective is to quantify the vertical profiles of the radar and derived microphysical variables and their differences between the three types of weather systems: continental MCSs, marine MCSs, and tropical cyclones. We anticipate this study will comprise a needed climatology which can serve as a reference against which the cloud models' outputs can be evaluated.

1.1. Radar Microphysical Retrieval Algorithms

The radar retrieval equations for computing microphysical variables in rain and ice which we utilize in our study can be found in Ryzhkov and Zrnic (2019, Chapter 11), Ryzhkov et al. (2020), Bukovcic et al. (2018, 2020), and Carlin et al. (2021). These equations are listed herein.

For radar microphysical retrievals in pure rain, the following formulas for LWC, median volume diameter D_0, and total number concentration of raindrops N_t have been used:

$$LWC = 1.38 \times 10^{-3} \times 10^{(0.1Z - 2.43Z_{DR} + 1.12Z_{DR}^2 - 0.176Z_{DR}^3)}, \quad (1)$$

$$D_0 = 0.717 + 1.48Z_{DR} - 0.725Z_{DR}^2 + 0.171Z_{DR}^3, \quad (2)$$

$$\log(N_t) = -2.37 + 0.1Z - 2.89Z_{DR} + 1.28Z_{DR}^2 - 0.213Z_{DR}^3, \quad (3)$$

where LWC is expressed in g m^{-3}, D_0 is in mm, N_t is in L^{-1}, Z is in dBZ, and differential reflectivity Z_{DR} is in dB. Equations 1 and 3 have been derived using simulations based on a large disdrometer dataset in Oklahoma and Equation 2 was suggested by Brandes et al. (2004). It has to be mentioned that the median volume diameter of raindrops D_0 is quite close to its mean volume diameter D_m which is the ratio of the fourth and third moments of the raindrop size distribution:

$$D_0 = \frac{3.67 + \mu}{4 + \mu} D_m, \quad (4)$$

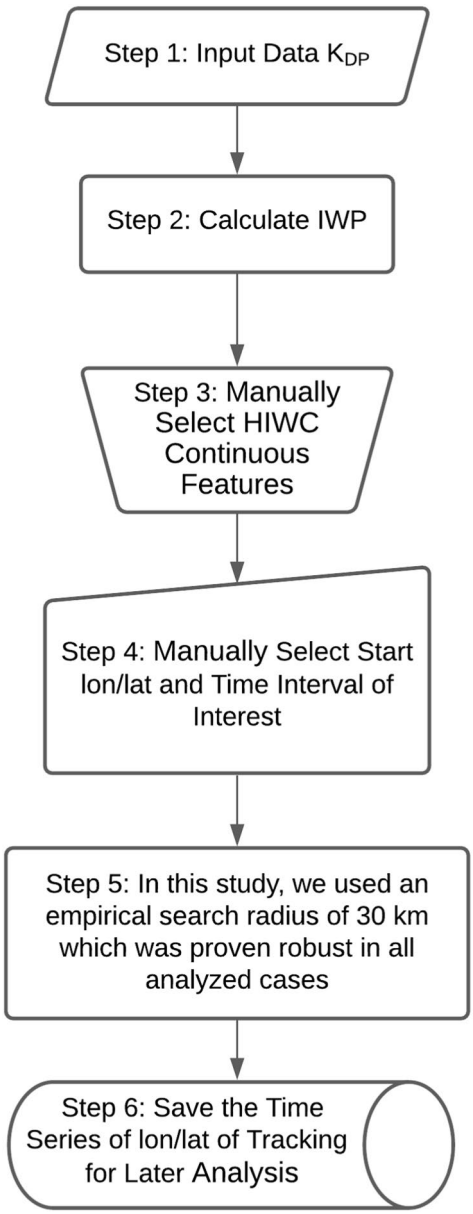

Figure 3. Flowchart of a tracking procedure for HIWC.

where μ is the shape factor of the gamma size distribution.

The errors of the estimators Equations 1–3 are specified in Ryzhkov et al. (2020). The fractional standard deviation (FSD) of the LWC estimate is about 35% if LWC varies from 0.1 to 1.0 g m^{-3}. The FSD of the D_0 estimate is about 10%. For the majority of DSDs the standard deviation of the $\log(N_t)$ estimate is about 0.3. However, it can be larger for very high ($\log(N_t) > 0$) and very low ($\log(N_t) < -1$) total concentrations of raindrops.

Two recently proposed sets of polarimetric relations for determination of IWC and D_m in ice are used in our analysis. The first set of equations utilizes a combination of the specific differential phase K_{DP} and differential reflectivity Z_{dr} expressed in a linear scale ($Z_{dr} = 10^{(0.1Z_{DR})}$) or reflectivity difference $Z_{dp} = Z\left(1 - Z_{dr}^{-1}\right)$ where Z is expressed in linear units ($mm^6\ m^{-3}$):

$$IWC\left(K_{DP}, Z_{dr}\right) = 4.0 \times 10^{-3} \frac{K_{DP}\lambda}{1 - Z_{dr}^{-1}}, \tag{5}$$

and

$$D_m\left(K_{DP}, Z_{dp}\right) = -0.1 + 2.0\left(\frac{Z_{dp}}{K_{DP}\lambda}\right)^{1/2}, \tag{6}$$

In Equation 5 and 6, λ is the radar wavelength in mm.

Another set of relations does not utilize Z_{dr} or Z_{dp} and uses a combination of K_{DP} and Z:

$$IWC = 3.3 \times 10^{-2}(K_{DP}\lambda)^{0.67} Z^{0.33}, \tag{7}$$

and

$$D_m = 0.67\left(\frac{Z}{K_{dp}\lambda}\right)^{1/3}, \tag{8}$$

In Equation 5–8, Z is expressed in linear units. The relations (5)–(8) were derived assuming that the particles are the Rayleigh scatterers with their density inversely proportional to the equivolume diameter D_e

$$\rho_s = \alpha_0 f_{rim} D_e^{-1}, \tag{9}$$

where α_0 is a constant and f_{rim} is the riming factor changing from 1 for unrimed ice to 5 for heavily rimed ice.

The advantage of the estimates (5) and (6) is that they are practically insensitive to the variability of the ice particles' shapes and orientations. However, they are very sensitive to possible errors in the Z_{dr} measurements, particularly at lower values of Z_{DR}. For this reason, Equations 5 and 6 are utilized if $Z_{DR} > 0.4$ dB (Carlin et al., 2021). Otherwise, IWC and D_m are estimated from Equations 7 and 8 that do not contain differential reflectivity. The inherent deficiency of these relations is that they are not immune to the variability of the particles' shapes and orientations. On the other hand, the $D_m(K_{DP},Z)$ estimate is not affected by the changes in the snow density or riming factor f_{rim}, whereas the relation $D_m(K_{DP},Z_{dp})$ is.

There are many definitions of the characteristic size of ice hydrometeors which generally have a nonspherical shape. The retrieval formulas 6 and 8 have been derived for the mean volume diameter D_m defined as the ratio of the fourth and third moments of the distribution of the *equivolume diameters* D_e of ice particles with a spheroidal shape. In the analyses of in situ measurements with the microphysical probes, the moments of the distribution of

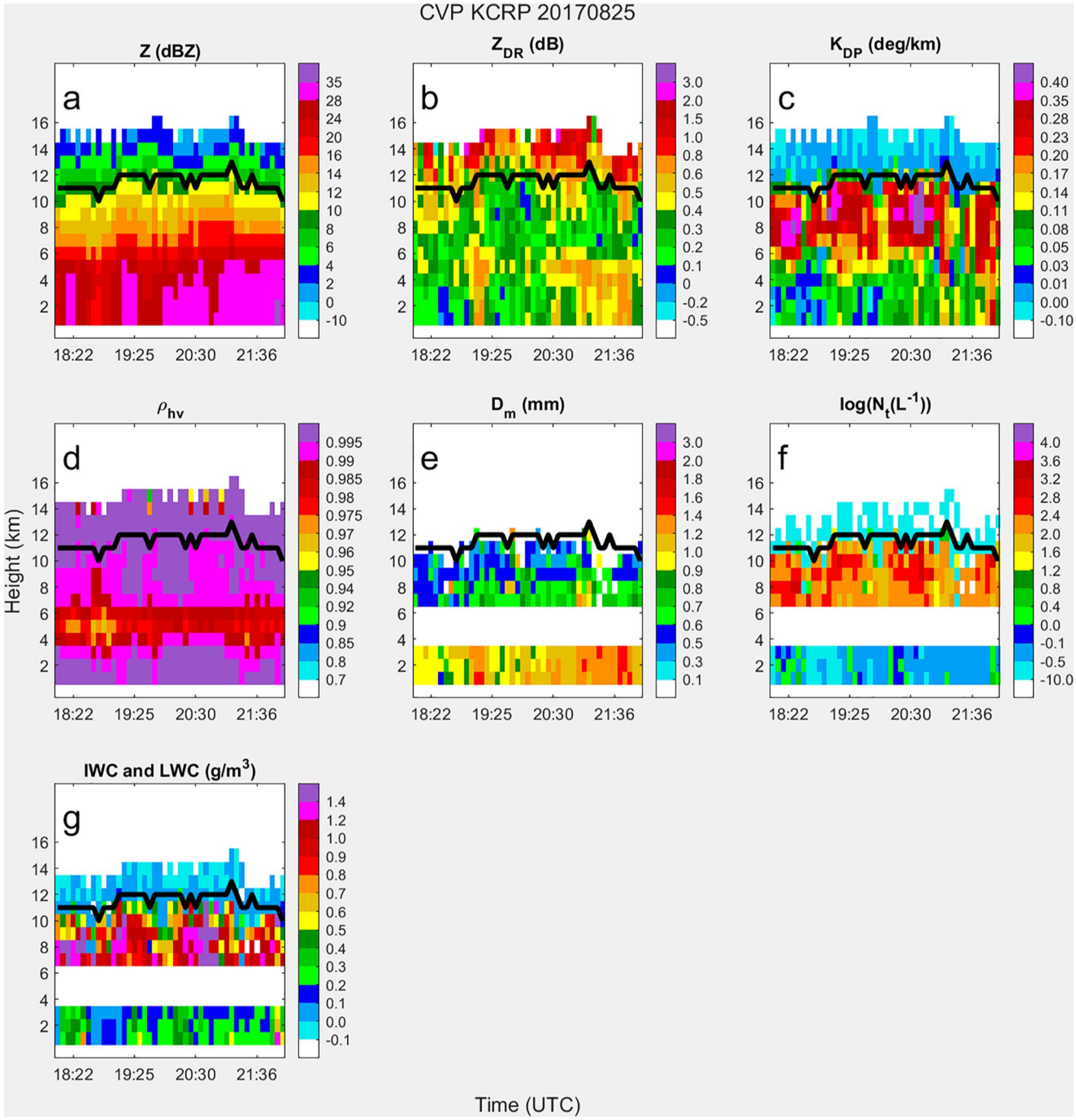

Figure 4. CVP time series between 1800 UTC to 2200 UTC 25 August 2017 near Corpus Christi, Texas (KCRP), WSR-88D radar. (a) Z, (b) Z_{DR}, (c) K_{DP}, (d) ρ_{hv}, (e) D_m, (f) N_t, (g), and IWC/LWC. Black line represents the 10 dB SNR contour and pixels over this line are not used for CFAD calculations.

maximal particle dimensions $D_{max} > D_e$ are usually quantified. This circumstance has to be taken into account in the comparison of the radar retrieved characteristic sizes and the ones obtained from in situ probes.

Once IWC is determined either from Equation (5) or Equation (7), the total number concentration N_t of ice particles larger than 0.1 mm can be computed as

$$\log(N_t) = 3.39 + 2\ \log(IWC) - 0.1Z(dBZ), \tag{10}$$

Table 1
List of Events and WSR-88D Radars Used for Analysis

Type			
Continental MCSs	Date	UTC	NEXRAD
MCS	11 June 2018	0300–1000	KMBX
MCS	23 June 2018	0400–1100	KTLX
MCS	2 June 2018	0400–1200	KOAX
MCS	26 June 2019	0300–0800	KTWX
MCS	27 June 2019	0700–1200	KBIS
MCS	27 June 2019	1400–1900	KMPX
MCS	27 June 2019	1800–2300	KARX
MCS	30 June 2019	0900–1500	KDLH
MCS	6 June 2019	0400–0800	KDYX
MCS	15 June 2019	0500–1100	KICT
MCS	15 June 2019	0200–0700	KDDC
MCS	24 June 2019	0100–1000	KLZK
Marine MCSs			
MCS	1 February 2020	0100–2300	KBYX
MCS	7 February 2020	1000–1500	KBYX
MCS	14 May 2020	0200–0200(+1)	KBYX
MCS	25, May 2020	0400–1200	KBYX
MCS	3 June 2020	1000–1900	KBYX
MCS	4 June 2020	1000–1900	KBYX
MCS	18 June 2020	0000–0700	KBYX
MCS	22 February 2019	1800–1700(+1)	PGUA
MCS	12 September 2018	1500–0700(+1)	PHMO
MCS	23 July 2016	1700–1100(+1)	PHWA
Tropical cyclones			
MH (Harvey)	25 August 2017	1800–2200	KCRP
TS (Alberto)	28 May 2018	1400–2100	KEVX
MH (Michael)	10 October 2018	1500–2200	KEVX
TS (Imelda)	17 September 2019	1400–2400	KHGX
TS (Cindy)	21 June 2017	0000–0800	KLIX
MH (Irene)	27 August 2011	0000–2400	KMHX
MH (Dorian)	6 September 2019	0500–1100	KMHX
MH (Irma)	10 September 2017	0700–1600	KMLB, KBYX
TS (Cindy)	21 June 2017	0000–0800	KMOB
TS (Emily)	31 July 2017	0500–1100	KTBW
MH (Nate)	8 October 2017	0700–1800	KMOB, KEVX

Note. MH and TS labels indicate major hurricanes and tropical storms, respectively.

where N_t is in L^{-1}.

Since the retrievals (5)–(10) are based on the assumption that the ice/snow density is inversely proportional to the particle size, they are not applicable in the convective cores with strong updrafts where graupel or hail is present. Therefore, they are primarily valid in the stratiform parts of MCSs, peripheries of the tropical cyclones, and thunderstorm anvils. They also cannot be used in the melting layer (ML) filled with mixed-phase hydrometeors.

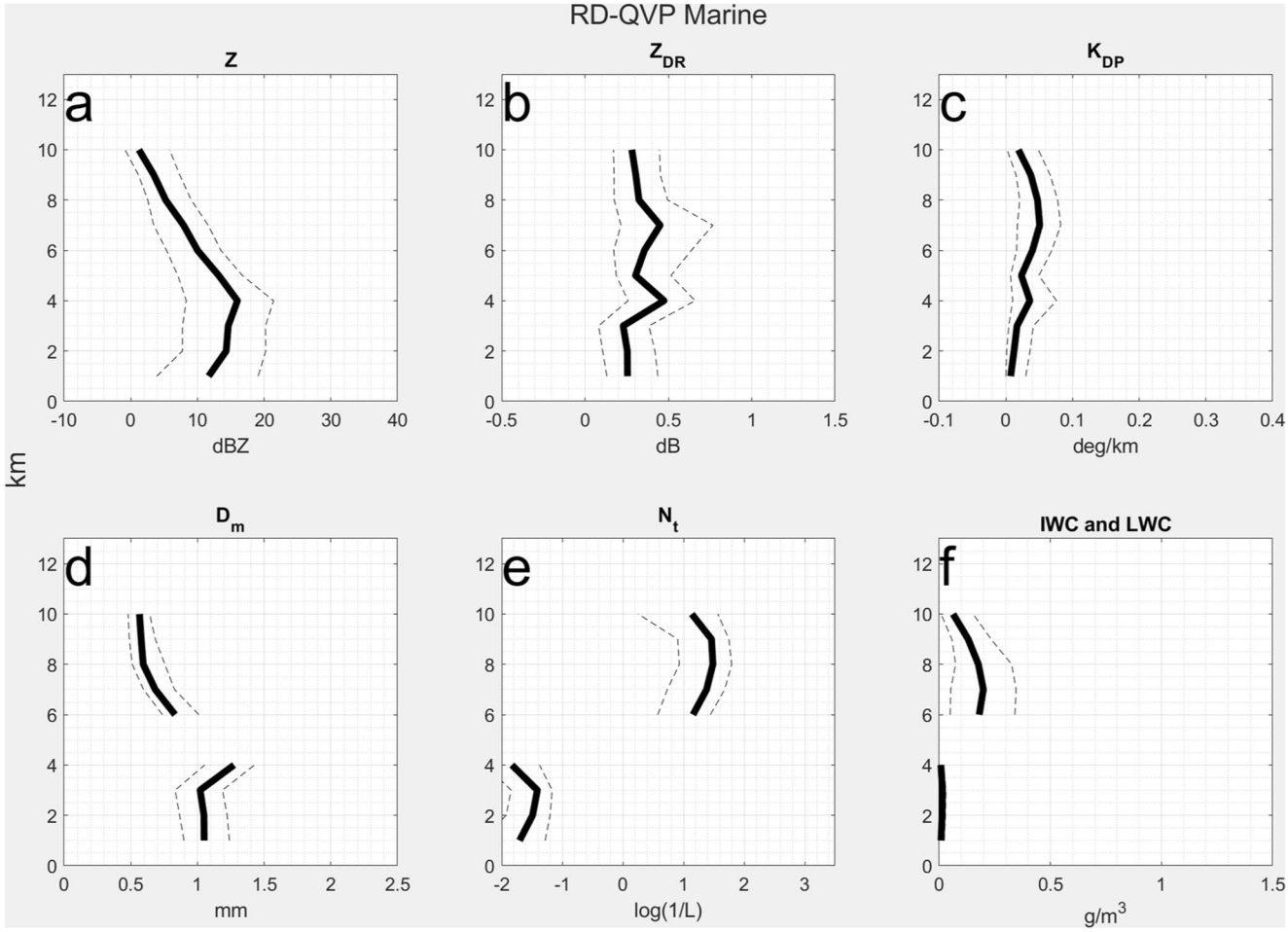

Figure 5. Median vertical profiles for the marine RD-QVP dataset: (a) Z, (b) Z_{DR}, (c) K_{DP}, (d) D_m, (e) N_t, and (f) IWC/LWC (solid lines). Dotted lines on the left and right hand sides of each solid line represent the corresponding 25th and 75th percentiles data.

The accuracy of the polarimetric ice retrievals is determined by the natural variability of the size distributions of ice, its shape, orientation, and density as well as the measurement errors of the polarimetric radar variables. Theoretical simulations assuming gamma size distribution with various shape factors μ indicate that the value of FSD for IWC estimated from Equation 5 is below 20% if $-1 < \mu < 1$, and IWC is slightly overestimated for $\mu < -1$ (Ryzhkov et al., 2020; Ryzhkov & Zrnic, 2019). For a given degree of riming f_{rim}, the FSD of the D_m estimate (6) is below 20%, but some adjustment of Equation 6 might be needed depending on f_{rim}. The error of the $\log(N_t)$ estimate varies between 0.7 and 1.0 (in log units). A more detailed discussion on the accuracy of the polarimetric retrievals (5)–(10) can be found in Ryzhkov and Zrnic (2019), Ryzhkov et al. (2020), and Bukovcic et al. (2018, 2020).

As mentioned earlier, one of the primary advantages of using K_{DP} is that it is proportional to the first moment of the size distribution, whereas Z is proportional to its fourth moment (if the inverse dependency of the density of snowflakes on their size is assumed) and is therefore disproportionally weighted by by a few largest ice particles. Another advantage of K_{DP} is that it is not biased by noise, attenuation, and radar miscalibration. On the other hand, the magnitude of K_{DP} in dry ice and snow is relatively small, particularly at longer radar wavelengths. Aggressive spatial averaging of K_{DP} and Z_{DR} implemented in the RD-QVP and CVP methodologies helps to reduce inherent noisiness of the K_{DP} and Z_{DR} estimates and the corresponding retrieval estimates. We also avoid using the retrievals in areas where $K_{DP} < 0.009°km^{-1}$ and the signal-to-noise ratio (SNR) is less than 10 dB. In our analysis, we use K_{DP} values obtained as the output of the standard WSR-88D differential phase processing briefly described in Ryzhkov, Giangrande, and Schuur (2005) and the spatial averaging of K_{DP} was applied

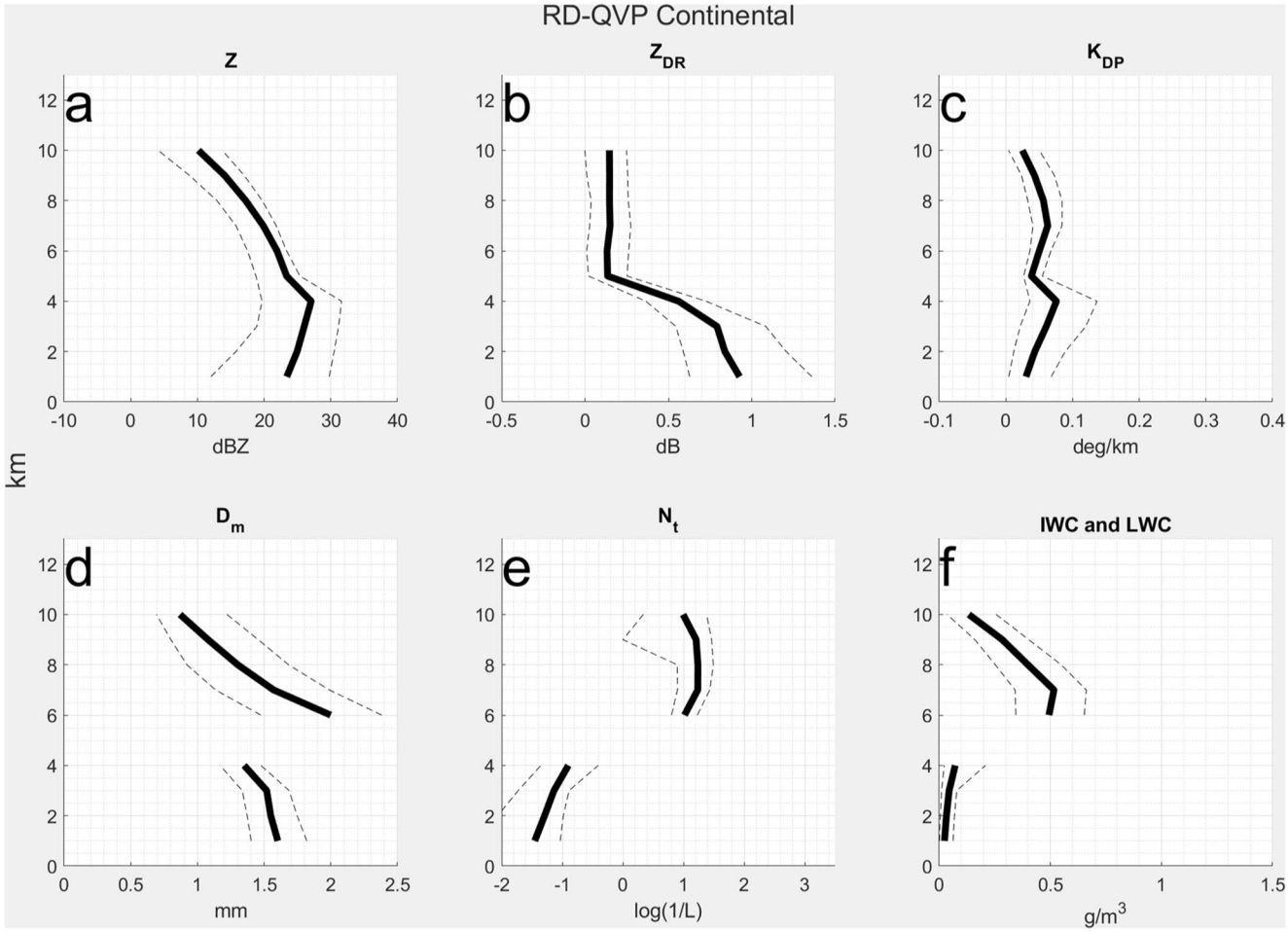

Figure 6. Same as in Figure 5, but for the RD-QVP statistics for continental MCSs.

according to the RD-QVP and CVP methodologies. Absolute calibration of differential reflectivity Z_{DR} was performed manually for each case and radar using the RD-QVP profiles of Z_{DR} and ensuring that the value of Z_{DR} is in the range of 0.1–0.2 dB in dry aggregated snow above the ML as instructed in Ryzhkov, Giangrande, Melnikov, and Schuur (2005).

The accuracy of the polarimetric retrievals in ice used in our study was evaluated experimentally using in situ aircraft measurements by Ryzhkov et al. (1998), Nguyen et al. (2019), and Murphy et al. (2020) and surface measurements by Bukovcic et al. (2018, 2020). Although the results are encouraging, we continue testing and refining the retrieval relations in ice. However, at the moment, we have enough confidence in the retrievals (5)–(10) to utilize them in our climatological study presented in this article.

Alternative statistical polarimetric retrieval methods in ice were recently suggested by Kedzuf et al. (2021) and Munchak et al. (2021) which are also designed for estimation of IWC, D_m, and N_t for each ice species and their mixtures along the radials of polarimetric radar data. Kedzuf et al. (2021) proposed the iterative stochastic ensemble Kalman filter approach and Munchak et al. (2021) used optimal estimation to solve for several parameters that describe PSD, relative contribution of pristine, aggregate, and rimed ice species, and the orientation distribution along an entire radial simultaneously. While these methodologies hold certain promises, they are very computationally intensive and their efficiency still needs to be investigated.

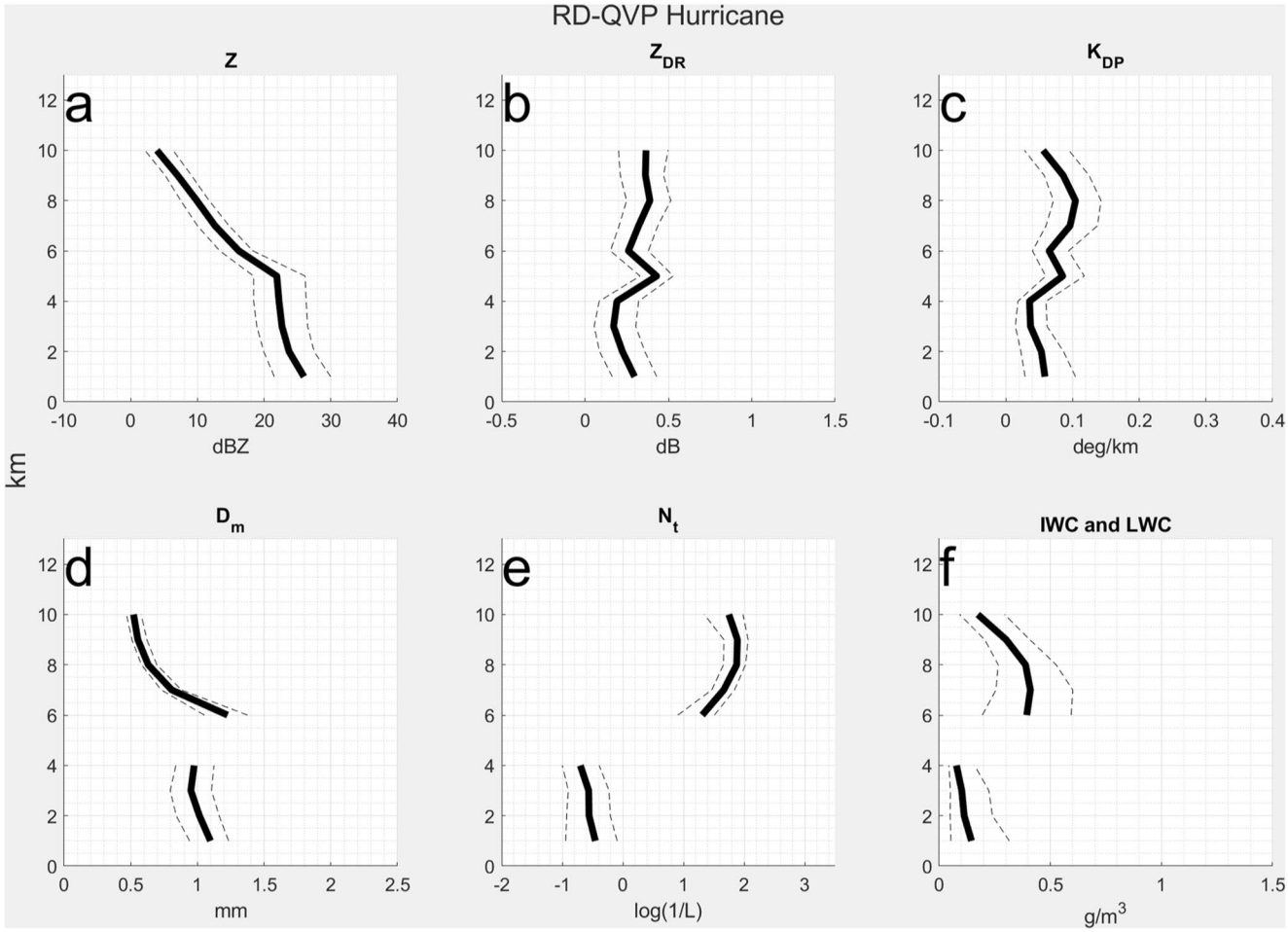

Figure 7. Same as in Figure 5 but for the hurricane RD-QVP statistics.

2. Methodology

In this study, we distinguish between two types of statistics of the vertical profiles of the radar and microphysical variables: the "background" and the "HIWC" statistics. The background statistic encompasses all stratiform parts of the clouds regardless of their IWC, whereas the "HIWC" statistics are built for the vertical columns in the clouds containing high IWC above the ML with ice water path (IWP; vertically integrated IWC) exceeding 4.5 kg m^{-2}. The two statistics require different methodologies for processing of the radar data. The RD-QVP technique is suitable for the background statistics approach because the data are analyzed in a 50 km—radius vertical column centered on the radar. The HIWC statistics require identification and tracking the HIWC areas within the storm which can be farther than 50 km from the radar and estimating vertical profiles in continuously moving columns containing high amount of ice. The CVP methodology is the best choice for this task.

2.1. RD-QVP Products

According to the original QVP methodology introduced in Kumjian et al. (2013) and Ryzhkov et al. (2016), vertical profiles of polarimetric radar variables are created by azimuthal averaging of the radar data in a full 360° circle at a single elevation angle usually selected between 10 and 20 . The data are presented in a height-time format which represents temporal evolution of the vertical structure of the storm with high vertical resolution. Tobin and Kumjian (2017) modified original QVP technique by suggesting the "range-defined" QVP (RD-QVP), which combines QVPs at multiple elevations using an inverse distance weighting technique. The RD-QVP technique uses radar data from the distances within 50 km from the radar at all available elevation angles.

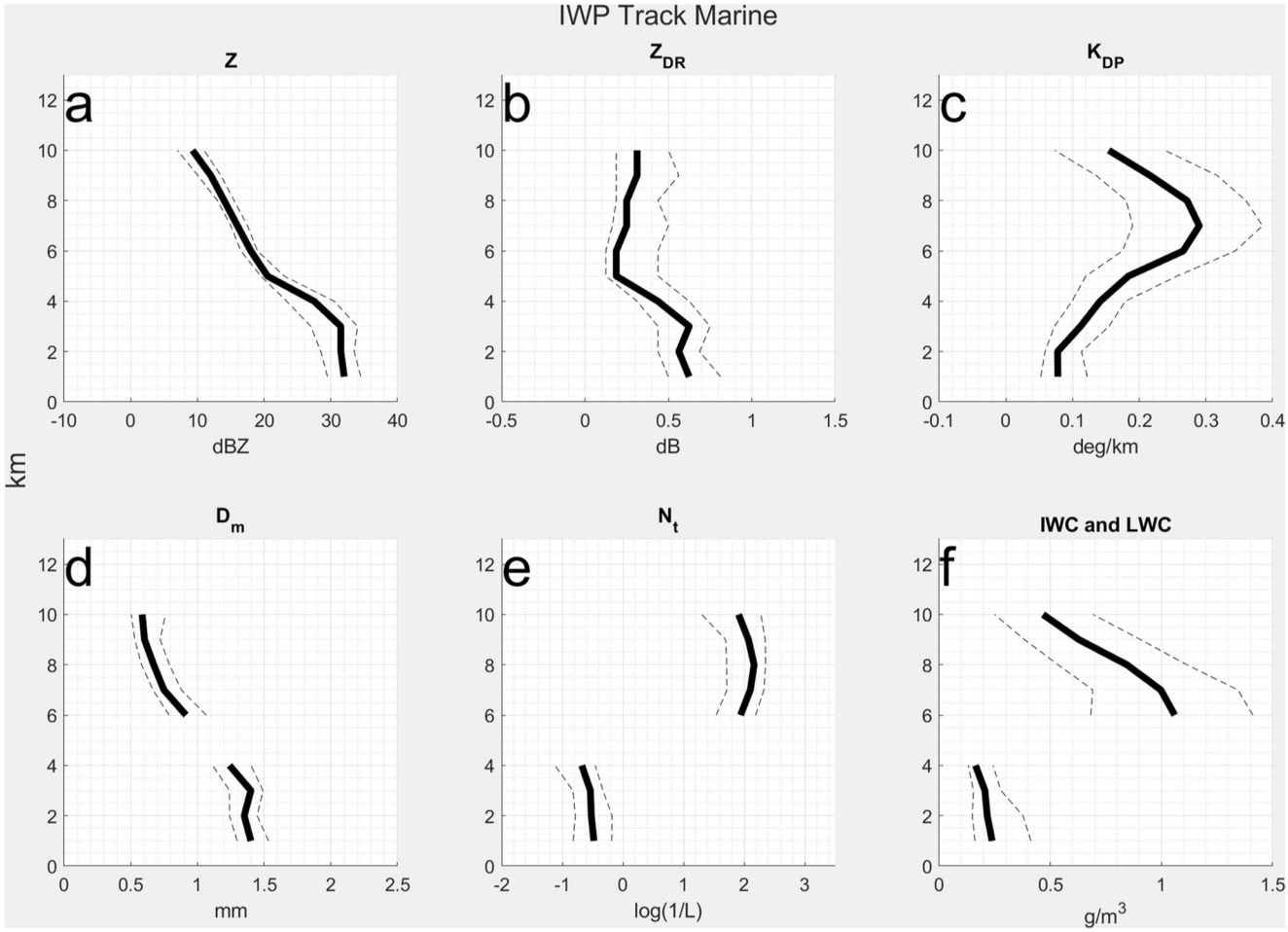

Figure 8. Median vertical profiles for the marine HIWC track dataset: (a) Z, (b) Z_{DR}, (c) K_{DP}, (d) D_m, (e) N_t, and (f) IWC/LWC. Dotted lines on the left and right hand sides of each solid line represent the corresponding 25th and 75th percentiles data.

An example of the RD-QVP product for Hurricane Harvey (2017) observed by the Corpus Christi, TX (KCRP) WSR-88D radar is displayed in Figure 1. The RD-QVPs of Z, Z_{DR}, K_{DP}, ρ_{hv} and LWC/IWC, D_m, and N_t are presented for the time period between 18 and 22 UTC on 25 August 2017. The RD-QVP technique captures a fine vertical structure of the storm with a clear signature of the ML in terms of Z_{DR} and ρ_{hv} between 4.5 and 5 km. Below the ML, a strong vertical gradient of K_{DP} exhibits a dominance of a classical warm rain process with rain rate increasing toward the surface as well as the raindrop size (see the Z_{DR} and D_m panels) due to a collision-coalescence process (Ryzhkov & Zrnic, 2019). In the ice part of the storm above the ML, radar reflectivity decreases with height very rapidly which is typical for tropical cyclones. Notable is a prominent increase of K_{DP} and Z_{DR} in the dendritic growth layer (DGL) centered at the −15°C altitude (8 km). High K_{DP} associated with low Z in the ice part of the storm is a classical feature of the tropical cyclones indicating relatively high concentration of small-size ice particles with quite substantial IWC (Nguyen et al., 2019; Ryzhkov & Zrnic, 2019).

Commonly used IWC(Z) relations tend to underestimate IWC in the majority of tropical storms (Ryzhkov & Zrnic, 2019). A frequently utilized IWC(Z) relation of Hogan et al. (2006).

$$IWC = 0.02 \times 10^{-0.02T} Z^{0.6}, \tag{11}$$

where T is the temperature in °C, yields IWC = 0.32 g m^{-3} at the height of 8 km where K_{DP} reaches its maximum and Z is only 15 dBZ. The corresponding polarimetric estimator (5) gives the IWC value of about 0.7 g m^{-3}, that is, more than two times larger. A combination of high K_{DP} and low Z signifies smaller sized ice particles accord-

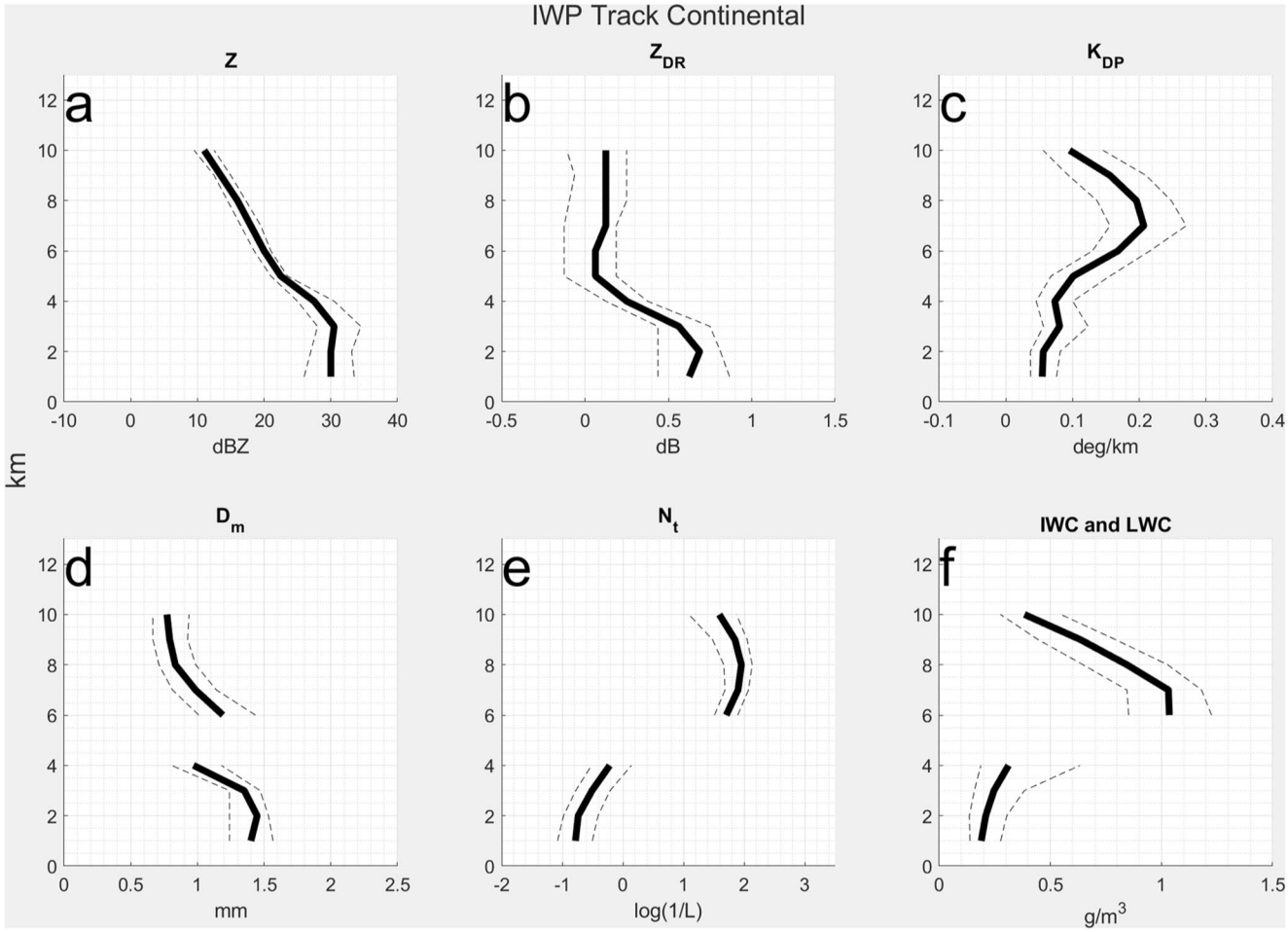

Figure 9. Same as in Figure 8, but for the continental HIWC statistics.

ing to Equation 6 or Equation 8. Indeed, the mean volume diameter D_m is only about 0.5 mm and its total number concentration reaches values over 100 L^{-1} at the same height.

The layer between 4 and 6 km centered on the ML is left blank in the microphysical QVP panels because our polarimetric retrievals are not designed for mixed-phase particles. The retrievals are less reliable in areas of low signal-to-noise ratio (SNR). The contours of SNR = 10 dB are overlaid in black in Figure 1. It is obvious that the retrieval estimates become erratic near the top of the storm where SNR < 10 dB. Therefore, we will use only the radar data with SNR > 10 dB for our quantitative analysis.

2.2. HIWC CVP Products

In order to identify the HIWC areas, the WSR-88D radar data are first converted into the Cartesian 3D format with a vertical resolution of 0.3 km and horizontal resolution of 0.005° in terms of latitude and longitude. Then a horizontal field of the IWP is generated as shown in the example illustrated in Figure 2 from the same Hurricane Harvey. In our study, we estimated IWP by integrating the vertical profile of K_{DP} starting from the altitude 6 km as

$$IWP = 3.2 \int_{H=6km} K_{DP}\, dh, \tag{12}$$

assuming a simplified relation

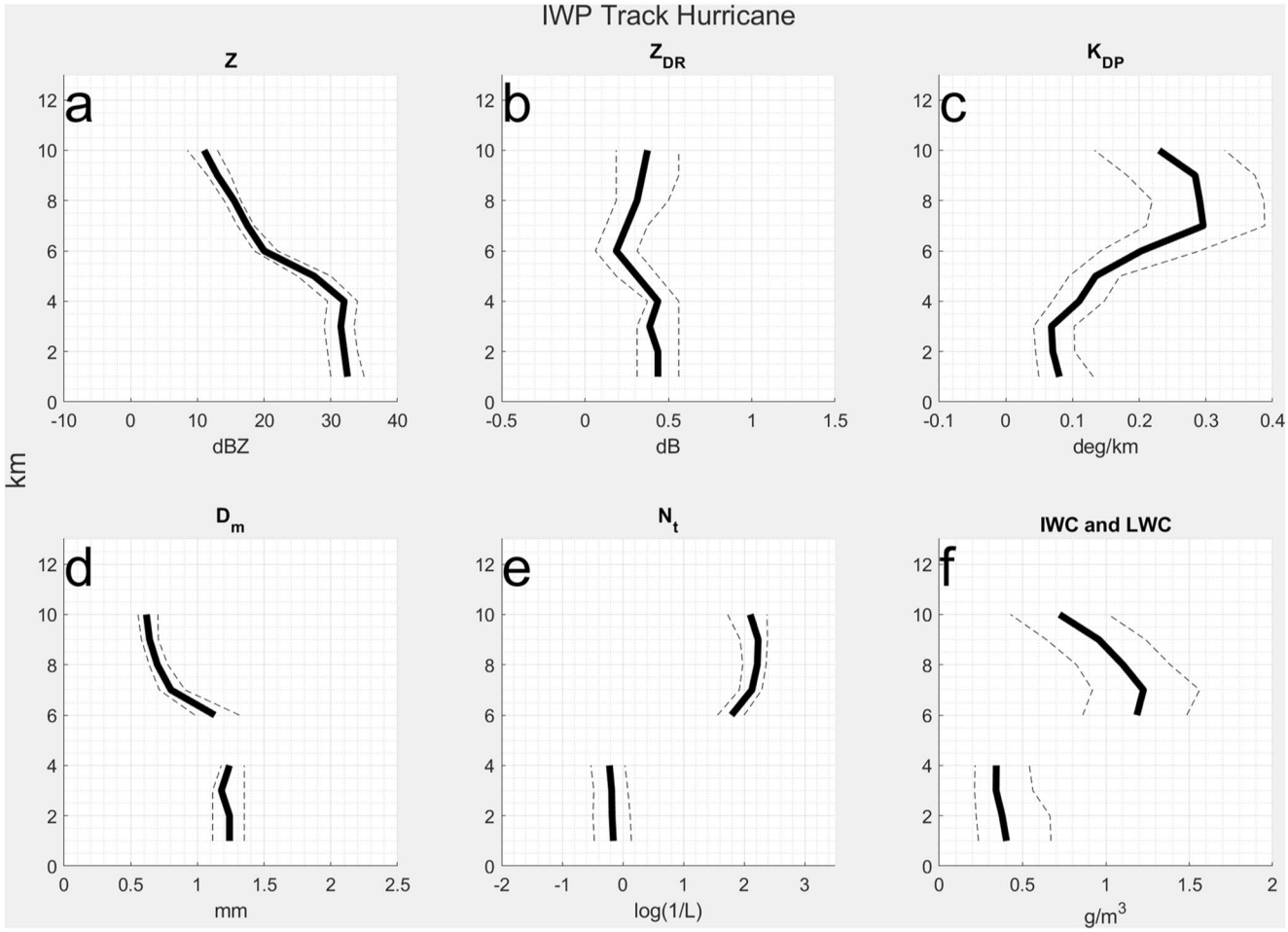

Figure 10. Same as in Figure 8, but for the hurricane HIWC statistics.

$$IWC = 3.2K_{DP}, \tag{13}$$

valid at S band (Ryzhkov et al., 1998; Ryzhkov & Zrnic, 2019). In Equations12 and 13, IWP is expressed in kg m^{-2} and IWC is in g m^{-3} Equation 13 is different from the more accurate polarimetric relations 5 and 7 and we opt to use it for classification purpose only due to its simplicity (steps 1 and 2 in Figure 3 where a flowchart of the tracking method used in our study is displayed).

Because our retrievals (Equations 5–10) are not applicable in deep convective cores, we avoid estimating IWP and performing our microphysical retrievals within vertical columns where radar reflectivity Z exceeds 30 dBZ at altitudes above 6 km.

The HIWC areas in the IWP maps are identified using the IWP threshold value equal to 4.5 kg m^{-2}. We selected this threshold from the higher end of the IWP distributions in the thunderstorm anvils reported by Tian et al. (2018).

The tracking of the HIWC areas was done in a semi-subjective manner. For each examined storm, we first went through the IWP map time series and picked up continuous HIWC features as shown in the Supporting Information (Step 3 in Figure 3). Then we manually pinpointed the starting longitude and latitude for tracking. The starting and ending time steps were also subjectively selected based on the IWP map as mentioned above (Step 4 in Figure 3). The next step was to track HIWC centers between time steps, which was done by searching for the maximum IWP near the HIWC center point from the previous tracking step. In this study, we used an empirical search radius of 30 km which was proven robust in all analyzed cases (Step 5 in Figure 3). The tracking procedure runs in the Cartesian coordinates and outputs the lon/lat of HIWC centers at each time step. These locations were

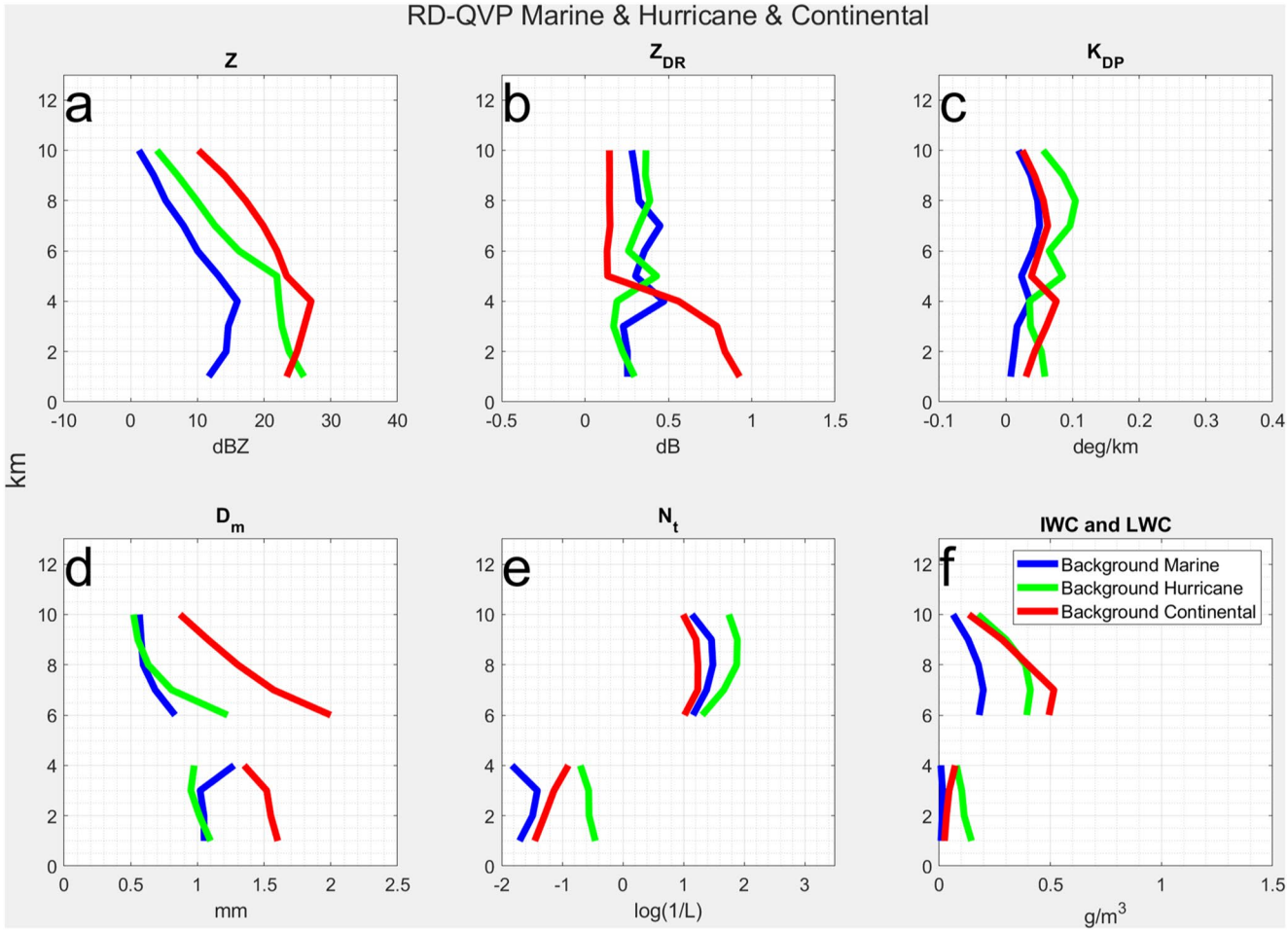

Figure 11. Median vertical profiles for the RD-QVP dataset: (a) Z, (b) Z_{DR}, (c) K_{DP}, (d) D_m, (e) N_t, and (f) IWC/LWC. Blue, green, and red lines represent marine, tropical cyclone, and continental profiles, respectively.

used for generation of the columnar vertical profiles (CVP) of Z, Z_{DR}, K_{DP}, and ρ_{hv} and retrieval calculations, which will be detailed next (Step 6 in Figure 3).

Vertical profiles of the radar and microphysical variables associated with a moving HIWC vertical column were obtained using the CVP technique described by Murphy et al. (2020) and Hu et al. (2020). In our study, a radial extension of the CVP column is 20 km while its azimuthal size is 20°. That is, the horizontal extent of the CVP column is much smaller than the one of the radar-centered RD-QVP column which allows to better focus on the HIWC areas which are often relatively small. Both CVP and RD-QVP average data azimuthally, except CVP mean calculation utilizes 20 points (20° azimuthal size with 1° resolution) at each vertical level in this study. Because K_{DP} in ice at S band is quite low and noisy, quite aggressive spatial averaging at any height level within the CVP column is needed. This dictates the choice of a horizontal size of the CVP columns which is sufficiently large (although smaller than the horizontal size of the RD-QVP column). An example of the HIWC CVP time series for Hurricane Harvey and the time interval between 18 and 22 UTC is shown in Figure 4. A tracking snapshot of the HIWC column is displayed in Figure 2. This column was relatively close to the eye of Hurricane Harvey when it landed near Corpus Christi. The distance between the center of a HIWC column and the KCPR WSR-88D radar varied between 93 and 108 km during this time period. It is no surprise that the vertical resolution of the CVP profiles is worse than that of the RD-QVP profiles, given that the CVP column was much father from the radar. As a result, a signature of the ML is barely visible in the ρ_{hv} panel and is indistinguishable in the vertical cross sections of Z and Z_{DR}. Nevertheless, the CVP series displays persistently high K_{DP} at the altitudes above 6 km associated with relatively low Z, as expected. The corresponding values of IWC generally exceed

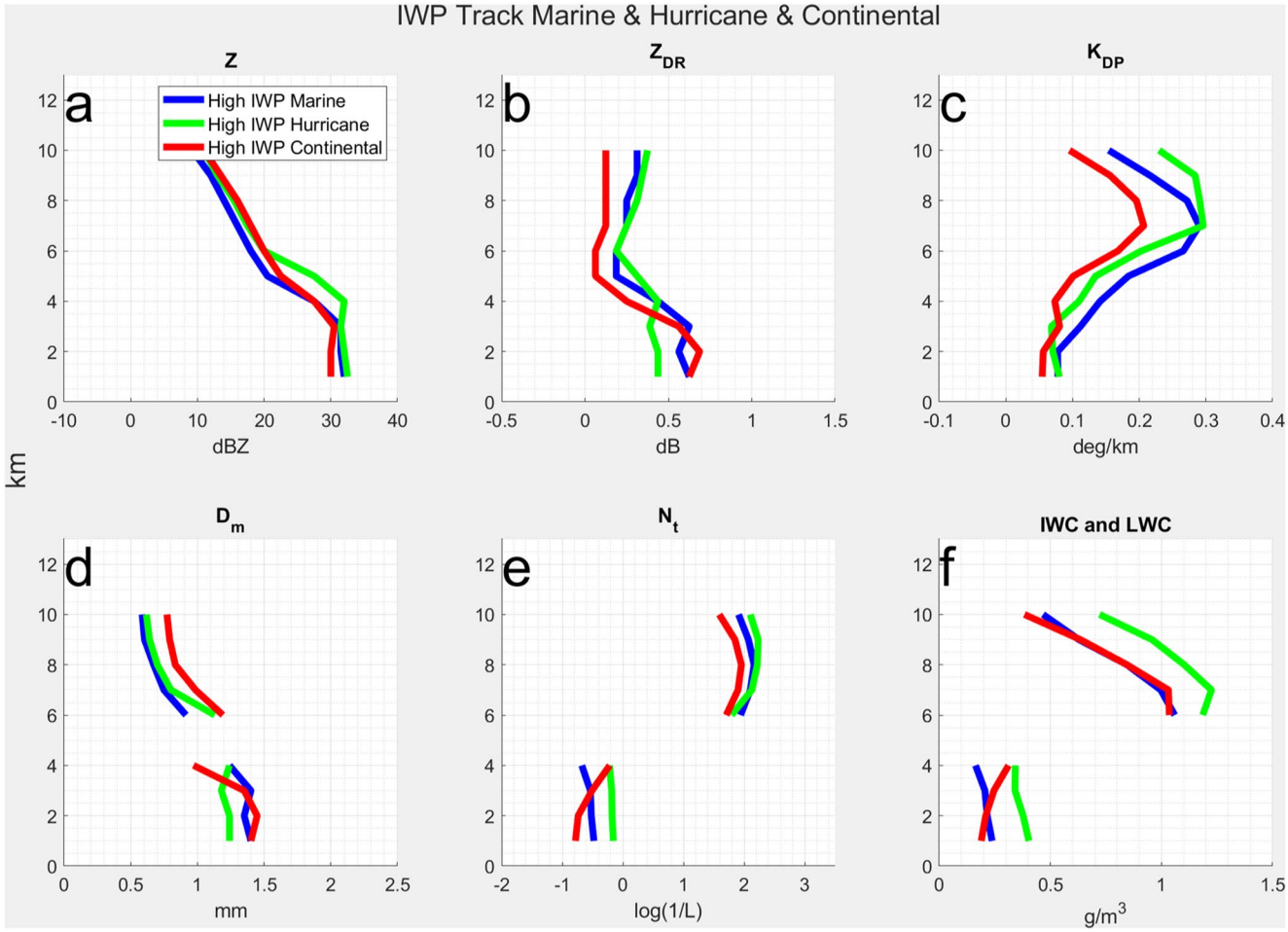

Figure 12. Median vertical profiles for the HIWC track dataset: (a) Z, (b) Z_{DR}, (c) K_{DP}, (d) D_m, (e) N_t, and (f) IWC/LWC. Blue, green, and red lines represent marine, tropical cyclone, and continental profiles.

1 g m^{-3} occasionally reaching 1.4 g m^{-3}, whereas D_m remains below 1 mm and N_t is consistently higher than 100 L^{-1}.

3. Dataset

Three types of storm systems have been investigated in this study: continental MCSs, marine MCSs, and land-falling tropical cyclones. A list of selected storms, their dates, and the names of WSR-88D radars is shown in Table 1. All storms' paths must overlap with at least one of the WSR-88D radar sites in order to be selected. For each case in Table 1, the CVPs along the HIWC tracking paths and RD-QVPs have been processed, saved, and displayed in the same fashion as shown in Figures 1 and 4.

4. Results

For every case, the radar variables and retrieved microphysical parameters are stacked in a height versus time format (as shown in Figures 1 and 4 for a given storm). The vertical profiles of radar variables and microphysical parameters are combined for each of the three categories of storms and the corresponding vertical median profiles and the profiles corresponding to the 25th and 75th percentiles of the variable distribution at every height level are displayed in Figures 5–10. The microphysical differences between the three categories of weather systems

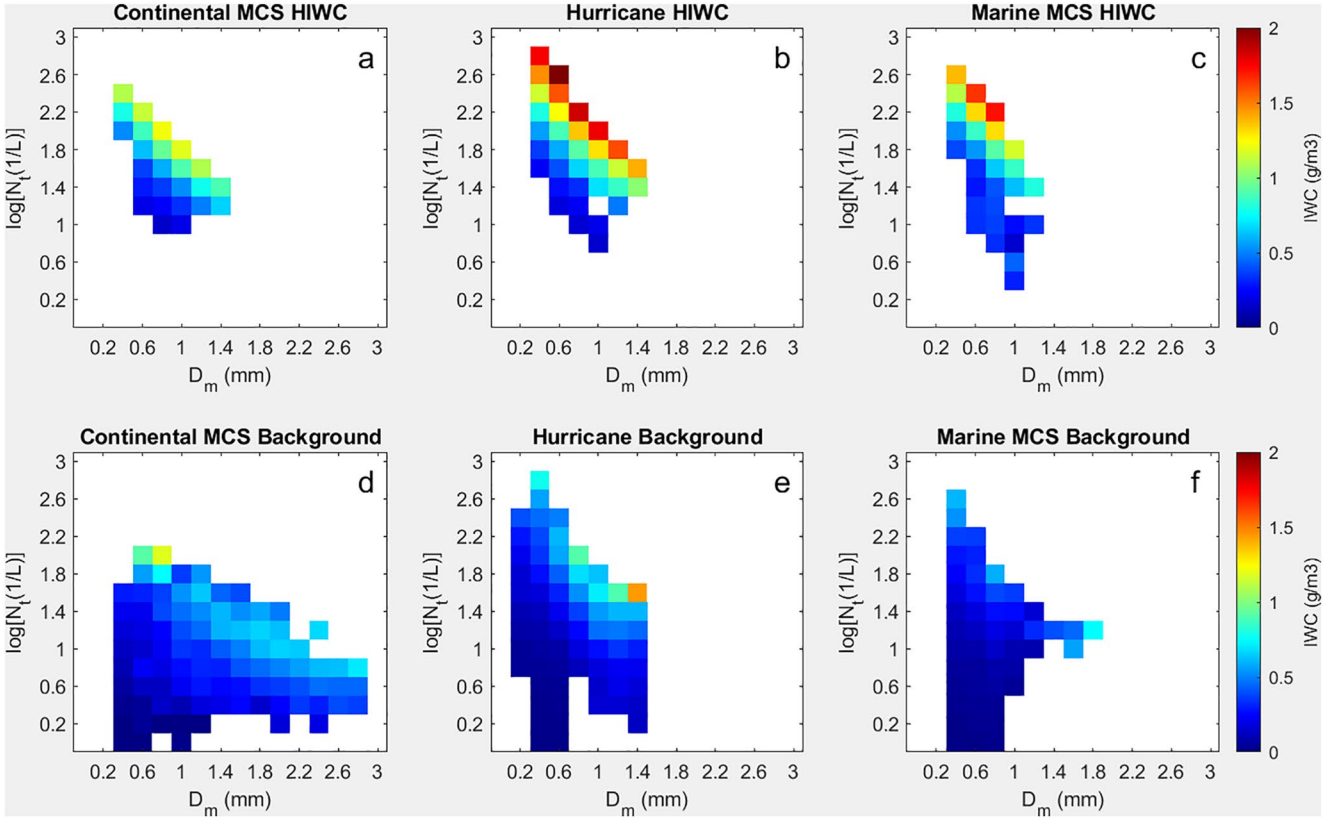

Figure 13. Distribution of the median values of IWC in the log(N_t) versus D_m plane for the HIWC and background statistics for three types of weather systems ([a] and [d] Continental MCS, [b] and [e] Hurricane, [c] and [f] Marine MCS).

are exhibited in Figure 11 and 12 where the vertical profiles of Z, Z_{DR}, K_{DP}, LWC/IWC, D_m, and N_t are compared separately for the RD-QVP and HIWC CVP analyses.

4.1. RD-QVPs

Vertical median profiles of radar reflectivity in Figure 11a show that Z in the ice parts of the storms is highest in the continental MCSs followed by the hurricanes. This is primarily due to the fact that the ice particles in continental MCSs are larger than those in marine MCSs and tropical cyclones. The reflectivity in the hurricanes is higher than in the continental storms only in rain next to the surface because of the strong collision/coalescence process at lower levels typical for warm rain in the tropics.

The difference in the vertical median profiles of Z_{DR} is quite dramatic with continental MCSs exhibiting the lowest values of Z_{DR} in ice above the ML and the highest values of Z_{DR} in rain below the ML (Figure 11b). Lower Z_{DR} in ice within the continental MCSs is attributed to larger size of the ice particles dominated by aggregated and possibly rimed snow which is generally characterized by lower bulk density and more spherical shape. Smaller size ice crystals with higher density and more anisotropic shape are prevalent in marine MCSs and tropical cyclones which explains higher values of Z_{DR} there. This pattern is also consistent with the highest K_{DP} in ice observed in the hurricanes (Figure 11c) because K_{DP}, being proportional to the first moment of the size distribution of ice, is mainly determined by the smallest ice particles in the size spectrum which have higher density and more nonspherical shape. Larger size snowflakes above the ML end up as larger raindrops after melting and, therefore, significantly higher values of Z_{DR} observed in the continental MCSs. Lower Z and higher K_{DP} in the ice portions of hurricanes signify smaller ice particles compared to the continental MCSs. Indeed, the mean volume diameter D_m is generally proportional to a cubic root of the ratio of Z and K_{DP} according to Equation 8. This feature is clearly illustrated by the vertical profiles of the median values of D_m in Figure 11d. In the continental storms, D_m in ice is almost two times higher than in the marine events. For a given IWC, the total number concen-

tration N_t of ice is higher in tropical storms because Z is lower—see Figure 11e. Larger D_m in ice aloft correspond to larger median values of D_m in rain for the continental MCSs, whereas a higher concentration of ice in tropical storms results in a higher concentration of raindrops below the ML. It is interesting that the median values of IWC are very comparable in the continental and tropical cases.

4.2. HIWC CVPs

Similar conclusions, with a few exceptions, can be drawn from the analysis of the HIWC CVP statistics (Figure 12). As expected, the HIWC areas are characterized by much higher K_{DP} in ice with the maximal median value reaching 0.3°km^{-1} in the tropical cyclones and marine MCSs. The corresponding values of IWC are also about three times higher than in the "background" RD-QVP statistics. It is not surprising that the radar reflectivity in ice is significantly higher in the HIWC regions of the tropical storms compared to their background because of much larger amount of ice aloft. Note that the vertical profiles of the median values of the mean volume diameter D_m of ice particles are very similar for the RD-QVP and HIWC CVP statistics. Therefore, a three-fold increase of IWC in the HIWC areas is achieved not by the increase of the size of ice particles but by the significant jump in their number concentration N_t (Figures 12d and 12e). Median values of N_t exceed 100 L^{-1} above the ML in the HIWC regions and the values of N_t higher than 1,000 L^{-1} are quite common (Figure 12e). The retrieved vertical profiles of N_t in Figures 11 and 12 do not show the anticipated increase of N_t with height. This pattern is most likely caused by the loss of sensitivity of the radar to the particles less than 0.1 mm in size. In other words, although actual total concentration of ice may increase with height, a good portion of such particles becomes invisible to the radar because of their decreasing size.

It is interesting that the Z_{DR} values in ice are lower in the HIWC regions of the tropical storms compared to their "background" RD-QVP values. The high values of Z_{DR} in stratiform parts of the storms are commonly observed within the DGL centered at the altitude with temperature of about −15°C. Griffin et al. (2018) showed that the highest values of Z_{DR} are observed within the DGL in the storms with lower tops just exceeding the DGL levels so that the highly anisotropic dendrites or hexagonal plates locally generated in the DGL are not masked by a bulk of more "quasi-spherical" ice with irregular shape falling from aloft. No Z_{DR} enhancement in the DGL is usually observed in the storms with high cloud tops. Hence, we believe that this is likely the reason why Z_{DR} in ice is lower in the HIWC areas commonly characterized by high cloud tops.

5. Discussion

An alternative way to summarize the results of our analysis illustrated in Figures 11 and 12 is to show a distribution of the median value of IWC in the $\log(N_t) - D_m$ plane for the background and HIWC statistics and three types of weather systems (Figure 13). The median values of IWC were obtained for all $\log(N_t) - D_m$ pairs in every 0.2×0.2 bin in the $\log(N_t) - D_m$ plane. Figure 13 shows that the highest median values of IWC approaching 1.5–2 g m^{-3} are observed in the hurricanes and marine MCSs and these are primarily associated with the highest total number concentrations of ice N_t and smallest sizes of ice particle D_m (Figures 13b and 13c). The continental MCSs reveal quite different pattern with noticeably lower median values of IWC even for HIWC cases (Figures 13a and 13d). Some differences between the total number of 0.2×0.2 bins in the Figures 13a–13f can be explained by the size of statistics which is the largest for the continental MCS background events.

The radar microphysical retrieval techniques in ice are still in the process of evaluation and refinement using in situ microphysical airborne and surface observations. However, we believe that Equations 5–10 used in this study is a good first attempt because they produce results consistent with occasional in situ measurements in the proximity of the polarimetric radars (e.g., Murphy et al., 2020; Nguyen et al., 2019; Ryzhkov et al., 1998) and which are in a ballpark of the majority of airborne probes' measurements of IWC, D_m, and N_t reported in the literature (e.g., Finlon et al., 2019; Heymsfield et al., 2013, 2015, 2017; Huang et al., 2021; Leroy et al., 2017; McFarquhar et al., 2007; Stechman et al., 2020). Such measurements in the stratiform parts of the continental MCSs during the BAMEX, MC3E, and PECAN field campaigns are summarized by McFarquhar et al. (2007), Tian et al. (2016), Finlon et al. (2019), and Stechman et al. (2020). For example, Finlon et al. (2019) reported the values of IWC averaged over all altitudes at negative temperatures in ice varying between 0.3 and 0.8 g m^{-3}, the corresponding values of the median mass-weighted diameter (D_{mm}) from 1 to 2 mm, and N_t from 20 to

40 L^{-1} during MC3E. Stechman et al. (2020) showed similar ranges for these variables observed in BAMEX and PECAN: 0.4–0.8 g m^{-3} for IWC, 2.0–2.5 mm for D_{mm}, and 15–60 L^{-1} for N_t. The in situ aircraft measurements in tropical clouds during the HAIC-HIWC experiments in Darwin, Australia, and Cayenne. French Guiana show generally higher values of IWC and N_t and lower values of D_{mm} in ice compared to the continental midlatitude MCSs. Leroy et al. (2017) reported IWC varying from 0.5 to 2.5 g m^{-3} and D_{mm} in the range between 0.25 and 0.7 mm in the Darwin flights. Huang et al. (2021) found very similar ranges of IWC and D_m during the flights in Cayenne and noted quite high total number concentrations N_t between 100 and 200 L^{-1}. All these numbers are consistent with the results of our polarimetric retrievals illustrated in Figure 12 and demonstrate similar differences between tropical and continental clouds.

As mentioned before, our retrieved D_m is the ratio of the fourth and third moments of the size distribution of equivolume diameters which is different from D_{mm} or median volume (D_{mv}) size commonly estimated from in situ airborne microphysical probes which measure a maximal particle dimension. It can be easily shown that $D_{mm} = 0.79\ D_m$ and $D_{mv} = 1.09\ D_m$ for the exponential size distribution and particle aspect ratio 0.6. We again emphasize that our estimated number concentration N_t is only for particles with sizes larger than 0.1 mm.

Analysis of the underlying reasons for the microphysical differences between the three types of weather systems is beyond the scope of this article. We can only speculate that the difference in the aerosol concentrations and strengths of convective updrafts in the continental and marine systems might be responsible for their significant contrast in terms of the median size of ice particles and their number concentration. We notice that extended HIWC areas in the stratiform parts of the marine MCS or tropical cyclones with reflectivities lower than 30 dBZ are usually well connected to the convective cores which tells that a bulk of small ice might be advected from the convective updrafts where the processes of SIP take place. It is quite likely that ice splintering by raindrop freezing in the updrafts is the primary mechanism responsible for high ice concentration below the homogeneous freezing level in clouds with warm cloud base, especially in the marine convective clouds and in the tropics (Lawson et al., 2015). In the continental clouds with colder cloud bases, secondary ice is produced within the convective zone as a result of hail-snow and graupel-snow collisions. It can penetrate the stratiform area at heights of about 7–8 km, with further increases of concentration caused by sublimational breakup in decaying parts of the storm (Phillips et al., 2017). Finally, extremely large amounts of small ice crystals in cloud anvils can be a result of homogeneous freezing of small droplets forming in the course of in-cloud nucleation of ultra-small CCN in the upper parts of deep convective clouds and above the level of homogeneous freezing (Fan et al., 2018; Khain et al., 2012).

6. Conclusions

A climatology of the vertical profiles of polarimetric radar variables and retrieved microphysical parameters such as LWC/IWC, mean volume diameter D_m, and total number concentration N_t has been documented for three types of weather systems: continental MCSs, marine MCSs, and tropical cyclones. This climatology is built based on the analysis of the WSR-88D radar data for 13 continental, 10 marine MCSs, and 11 landfalling hurricanes using novel methodologies for processing and visualizing the radar data such as RD-QVP and CVP. Separate statistics of the vertical profiles have been examined for the high IWC (HIWC) areas in the storms and compared with their "background" environment.

An overarching conclusion of the study is that marine MCSs and tropical cyclones are characterized by smaller size ice in higher concentration compared to the continental MCSs. We believe that this is a new result because we are not aware of any systematic comparisons of the microphysical properties of ice in the tropical and continental storms performed in the previous studies. HIWC areas is primarily caused by a strong jump in a number concentration of ice particles rather than the increase of their size compared to the "background" environment. This may point to the homogeneous nucleation of excessive amounts of supercooled droplets and/or SIP as the possible origins of HIWC. We emphasize that our radar retrieval techniques are valid mainly in the stratiform parts of the storm systems where graupel and hail are usually absent. Therefore, the reported results of the microphysical retrievals are representative of the storm areas where radar reflectivity in ice does not exceed 30 dBZ.

The climatology presented in this study can be used as an observational reference for cloud models' evaluation and optimization of their microphysical parameterization.

Conflict of Interest

The authors declare no conflicts of interest relevant to this study.

Data Availability Statement

Data used here is obtained from National Centers for Environmental Information (https://www.ncdc.noaa.gov/data-access).

Acknowledgments
Funding was provided by NOAA/Office of Oceanic and Atmospheric Research under NOAA-University of Oklahoma Cooperative Agreement #NA16OAR4320115, U.S. Department of Commerce, and by the U.S. National Weather Service, Federal Aviation Administration, and Department of Defense program for modernization of NEXRAD radars. Additional funding came from the Department of Energy grant DE-SC0018967. Our special thanks are extended to Dr. Pengfei Zhang who provided technical assistance in processing of polarimetric radar data.

References

Brandes, E., Zhang, G., & Vivekanandan, J. (2004). Drop size distribution retrieval with polarimetric radar: Model and application. *Journal of Applied Meteorology and Climatology*, *43*, 461–475. https://doi.org/10.1175/1520-0450(2004)043<0461:DSDRWP>2.0.CO;2

Bringi, V., & Chandrasekar, V. (2001). *Polarimetric Doppler weather radar* (p. 636). Cambridge University Press.

Bringi, V., Williams, C., Thurai, M., & May, P. (2009). Using dual-polarized radar and dual-frequency profiler for DSD characterization: A case study from Darwin, Australia. *Journal of Atmospheric and Oceanic Technology*, *26*, 2107–2122. https://doi.org/10.1175/2009jtecha1258.1

Bukovcic, P., Ryzhkov, A., & Zrnic, D. (2020). Polarimetric relations for snow estimation—Radar verification. *Journal of Applied Meteorology and Climatology*, *59*, 991–1009. 10.1175/JAMC-D-19-0140.1

Bukovcic, P., Ryzhkov, A., Zrnic, D., & Zhang, G. (2018). Polarimetric radar relations for quantification of snow based on the disdrometer data. *Journal of Applied Meteorology and Climatology*, *57*, 103–120. 10.1175/JAMC-D-17-0090.1

Bukovcic, P., Zrnic, D., & Zhang, G. (2017). Winter precipitation liquid-ice phase transitions revealed with polarimetric radar and 2DVD observations in central Oklahoma. *Journal of Applied Meteorology and Climatology*, *56*, 1345–1363. 10.1175/Jamc-D-16-0239.1

Cao, Q., Zhang, G., Brandes, E., Schuur, T., Ryzhkov, A., & Ikeda, K. (2008). Analysis of video disdrometer and polarimetric radar data to characterize rain microphysics in Oklahoma. *Journal of Applied Meteorology and Climatology*, *47*, 2238–2255. https://doi.org/10.1175/2008jamc1732.1

Carlin, J., Reeves, H., & Ryzhkov, A. (2021). Polarimetric observations and simulations of sublimating snow: Implications for nowcasting. *Journal of Applied Meteorology and Climatology*, *60*, 1035–1054. https://doi.org/10.1175/jamc-d-21-0038.1

Fan, J., Han, B., Varble, A., Morrison, H., North, K., Kollias, P., et al. (2017). Cloud-resolving model intercomparisons of an MC3E squall line case: Part I—Convective updrafts. *J. Geophys. Res. Atmos. 2017*, 122, 9351–9378. https://doi.org/10.1002/2017jd026622

Fan, J., Zhang, Y., Giangrande, S. E., Li, Z., Machado, L. A. T., Martin, S. T., et al. (2018). Substantial convection and precipitation enhancements by ultrafine aerosol particles. *Science*, *359*, 411 – 418. https://doi.org/10.1126/science.aan8461

Finlon, J., McFarquhar, G., Nesbitt, S., Rauber, R., Morrison, H., Wu, W., & Zhang, P. (2019). A novel approach for characterizing the variability in mass-dimension relationships: Results from MC3E. *Atmospheric Chemistry and Physics*, *19*, 3621–3643. https://doi.org/10.5194/acp-19-3621-2019

Fridlind, A., Ackerman, A., Grandin, A., Dezitter, F., Weber, M., Strapp, J., et al. (2015). High ice water content at low radar reflectivity near deep convection – Part I: Consistency of in situ and remote-sensing observations with stratiform rain column simulations. *Atmospheric Chemistry and Physics*, *15*, 11713–11728. https://doi.org/10.5194/acp-15-11713-2015

Griffin, E., Schuur, T., & Ryzhkov, A. (2018). A polarimetric analysis of ice microphysical processes in snow, using quasi-vertical profiles. *Journal of Applied Meteorology and Climatology*, *57*, 31–50. https://doi.org/10.1175/jamc-d-17-0033.1

Heymsfield, A. J., Bansemer, A., Heymsfield, G., & Fierro, A. O. (2009). Microphysics of maritime tropical convective updrafts at temperatures from −20° to −60°. *Journal of the Atmospheric Sciences*, *66*, 3530–3562. https://doi.org/10.1175/2009JAS3107.1

Heymsfield, A. J., Bansemer, A., Poellot, M., & Wood, N. (2015). Observations of ice microphysics through the melting layer. *Journal of the Atmospheric Sciences*, *72*, 2902–2928. https://doi.org/10.1175/jas-d-14-0363.1

Heymsfield, A. J., Kramer, M., Wood, N., Gettleman, A., Field, P., & Liu, G. (2017). Dependence of the ice water content and snowfall rate on temperature, globally: Comparison of in situ observations, satellite active remote sensing retrievals, and Global Climate Model simulations. *Journal of Applied Meteorology and Climatology*, *56*, 189–215. https://doi.org/10.1175/jamc-d-16-0230.1

Heymsfield, A. J., Schmitt, C., & Bansemer, A. (2013). Ice cloud particle size distributions and pressure-dependent terminal velocities from in situ observations at temperatures from 0° to −86°C. *Journal of the Atmospheric Sciences*, *70*, 4123–4154. https://doi.org/10.1175/jas-d-12-0124.1

Hogan, R., Mittermaier, M., & Illingworth, A. (2006). The retrievals of ice water content from radar reflectivity factor and temperature and its use in evaluating a mesoscale model. *Journal of Applied Meteorology and Climatology*, *45*, 301–317. https://doi.org/10.1175/jam2340.1

Homeyer, C., & Bowman, K. (2017). *Algorithm description document for version 3.1 of the three-dimensional gridded NEXRAD WSR-88D radar (GridRad) dataset* (Technical Report 23). University of Oklahoma; Texas A&M University. Retrieved from https://gridrad.org/pdf/GridRad-v3.1-Algorithm-Description.pdf

Homeyer, C., Fierro, A., Schenkel, B., Didlake, A., McFarquhar, G., Ryzhkov, A., et al. (2021). Polarimetric signatures in landfalling tropical cyclones. *Monthly Weather Review*, *149*, 131–154. https://doi.org/10.1175/mwr-d-20-0111.1

Hu, J., Rosenfeld, D., Ryzhkov, A., & Zhang, P. (2020). Synergetic use of the WSR-88D radars, GOES-R satellites, and lightning sensors to study microphysical characteristics of hurricanes. *Journal of Applied Meteorology and Climatology*, *59*, 1051–1068. https://doi.org/10.1175/jamc-d-19-0122.1

Huang, Y., Wu, W., McFarquhar, G., Wang, X., Morrison, H., Ryzhkov, A., et al. (2021). Microphysical processes producing high ice water contents (HIWCs) in tropical convective clouds during the HAIC-HIWC field campaign. Evaluations of simulations using bulk microphysical schemes. *Atmospheric Chemistry and Physics*, *21*, 6919 – 6944. https://doi.org/10.5194/acp-21-6919-2021

Kalina, E. A., Matrosov, S. Y., Cione, J. J., Marks, F. D., Vivekanandan, J., Black, R. A., et al. (2017). The Ice Water Paths of Small and Large Ice Species in Hurricanes Arthur (2014) and Irene (2011), *J. Appl. Meteor. Climatol*, *56*, 1383–1404. https://doi.org/10.1175/jamc-d-16-0300.1

Kedzuf, N., Chiu, J., Chandrasekar, V., Biswas, S., Joshil, S., van Leeuwen, P., et al. (2021). Retrieving microphysical properties of concurrent pristine ice and snow using polarimetric radar observations. *Atmos. Meas. Tech.*, *14*, 6885 – 6904. https://doi.org/10.5194/amt-14-6885-2021

Kennedy, P. C., & Rutledge, S. A. (2011). S-band dual-polarization radar observations of winter storms. *Journal of Applied Meteorology and Climatology*, *50*, 844–858. https://doi.org/10.1175/2010jamc2558.1

Khain, A., Phillips, V., Benmoshe, N., & Pokrovsky, A. (2012). The role of small soluble aerosols in the microphysics of deep maritime clouds. *Journal of the Atmospheric Sciences*, *69*, 2787–2807. https://doi.org/10.1175/2011jas3649.1

Khain, A., & Pinsky, M. (2018). *Physical Processes in Clouds and Cloud Modeling*. Cambridge University Press, 626 pp.
Korolev, A., & Leisner, T. (2020). Review of experimental studies on secondary ice production. *Atmos. Chem. Phys.*, *20*, 11767 – 11797. https://doi.org/10.5194/acp-20-11767-2020
Kumjian, M. (2018). Weather Radars: *Weather radars. Remote Sensing of Clouds and Precipitation*, In C. Andronache (Ed.), Springer-Verlag, 15–63. https://doi.org/10.1007/978-3-319-72583-3_2
Kumjian, M., Khain, A., Benmoshe, N., Ilotoviz, E., Ryzhkov, A., & Phillips, V., (2014). The anatomy and physics of ZDR columns: Investigating a polarimetric radar signature with a spectral bin microphysical model. *Journal of Applied Meteorology and Climatology*, *53*, 1820 – 1843. https://doi.org/10.1175/jamc-d-13-0354.1
Kumjian, M., & Ryzhkov, A. (2009). Storm-relative helicity revealed from polarimetric radar measurements. *Journal of the Atmospheric Sciences*, *66*, 667 – 685. https://doi.org/10.1175/2008jas2815.1
Kumjian, M., & Ryzhkov, A. (2010). The impact of evaporation on polarimetric characteristics of rain. Theoretical model and practical implications. *Journal of Applied Meteorology and Climatology*, *49*, 1247–1267. https://doi.org/10.1175/2010jamc2243.1
Kumjian, M., & Ryzhkov, A. (2012). The impact of size sorting on the polarimetric radar variables. *Journal of the Atmospheric Sciences*, *69*, 2042–2060. https://doi.org/10.1175/jas-d-11-0125.1
Kumjian, M., Ryzhkov, A., Reeves, H., & Schuur, T. (2013). A dual-polarization radar signature of hydrometeor refreezing in winter storms. *Journal of Applied Meteorology and Climatology*, *52*, 2549–2566. https://doi.org/10.1175/jamc-d-12-0311.1
Lawson, R., Woods, S., & Morrison, H. (2015). The microphysics of ice and precipitation development in tropical cumulus clouds. *Journal of the Atmospheric Sciences*, *72*, 2429–2445. https://doi.org/10.1175/jas-d-14-0274.1
Leroy, D., Fontaine, E., Schwarzenboeck, A., Strapp, J. W., Korolev, A., McFarquhar, G., et al. (2017). Ice crystal sizes in high ice water content clouds. Part II: Statistics of mass diameter percentiles in tropical convection observed during the HAIC/HIWC project. *Journal of Atmospheric and Oceanic Technology*, *34*, 117–136. https://doi.org/10.1175/jtech-d-15-0246.1
Matrosov, S., & Heymsfield, A. (2017). Empirical relations between size parameters of ice hydrometeor populations and radar reflectivity. *Journal of Applied Meteorology and Climatology*, *56*, 2479–2488. https://doi.org/10.1175/jamc-d-17-0076.1
McFarquhar, G., & Heymsfield, A. (1996). Microphysical characteristics of three anvils sampled during the central equatorial Pacific experiment. *Journal of the Atmospheric Sciences*, *53*, 2401–2423. 10.1175/1520-0469(1996)053<2401:MCOTAS>2.0.CO;2
McFarquhar, G., Timlin, M., Rauber, R., Jewett, B., Grim, J., & Jorgensen, D. (2007). Vertical variability of cloud hydrometeors in the stratiform region of mesoscale convective systems and bow echoes. *Monthly Weather Review*, *135*, 3405–3428. https://doi.org/10.1175/mwr3444.1
Morrison, H., Milbrandt, J., Bryan, G., Ikeda, S., Tessendorf, S., & Thompson, G. (2015). Parameterization of cloud microphysics based on the prediction of bulk ice particle properties. Part II: Case study comparisons with observations and other schemes. *Journal of the Atmospheric Sciences*, *2015*(72), 312–339. https://doi.org/10.1175/jas-d-14-0066.1
Morrison, H., van Lier-Walqui, M., Fridlind, A., Grabowski, W., Harrington, J., Hoose, C., et al. (2020). Confronting the Challenge of Modeling Cloud and Precipitation Microphysics, *Journal of Advances in Modeling Earth Systems*, *12*, e2019MS001689. https://doi.org/10.1029/2019ms001689
Munchak, S., Schrom, R., Helms, C., & Tokay, A. (2021). Snow Microphysical Retrieval from the NASA D3R Radar During ICE-POP 2018, *Atmos. Meas. Tech. Discuss*. https://doi.org/10.5194/amt-2021-264
Murphy, A., Ryzhkov, A., & Zhang, P. (2020). Columnar vertical profiles (CVP) methodology for validating polarimetric radar retrievals in ice using in situ aircraft measurements. *Journal of Atmospheric and Oceanic Technology*, *37*, 1623–1642. https://doi.org/10.1175/jtech-d-20-0011.1
Nguyen, C., Wolde, M., & Korolev, A. (2019). Determination of ice water content (IWC) in tropical convective clouds from X-band dual-polarization airborne radar. *Atmospheric Measurement Techniques*, *12*, 5897–5911. https://doi.org/10.5194/amt-12-5897-2019
Phillips, V., Yano, J.-I., & Khain, A. (2017). Ice multiplication by break-up in ice-ice collisions. Part I: Theoretical formulation. *Journal of the Atmospheric Sciences*, *74*, 1705–1719. https://doi.org/10.1175/jas-d-16-0224.1
Protat, A., Strapp, J. W., Fontaine, E., Leroy, D., Schwarzenboeck, A., et al. (2016). The measured relationship between ice water content and cloud radar reflectivity in tropical convective clouds. *Journal of Applied Meteorology and Climatology*, *55*, 1707–1729. https://doi.org/10.1175/jamc-d-15-0248.1
Rosenfeld, D., & Woodley, W. (2000). Deep convective clouds with sustained supercooled liquid water down to -37.5°C. *Nature*, *405*, 440–442. https://doi.org/10.1038/35013030
Ryzhkov, A., Bukovcic, P., Murphy, A., Zhang, P., & McFarquhar, G. (2018). Ice microphysical retrievals using polarimetric radar data. *Paper presented at the 10th European Conference on Radar in Meteorology and Hydrology*.
Ryzhkov, A., Giangrande, S., Melnikov, V., & Schuur, T. (2005). Calibration issues of dual-polarization radar measurements. *Journal of Atmospheric and Oceanic Technology*, *22*, 1138–1155. https://doi.org/10.1175/jtech1772.1
Ryzhkov, A., Giangrande, S., & Schuur, T. (2005). Rainfall estimation with a polarimetric prototype of the WSR-88D radar. *Journal of Applied Meteorology*, *44*, 502–515. https://doi.org/10.1175/jam2213.1
Ryzhkov, A., Kumjian, M., Ganson, S., & Khain, A. (2013). Polarimetric radar characteristics of melting hail. Pt I: Theoretical simulations using spectral microphysical modeling. *Journal of Applied Meteorology and Climatology*, *52*, 2849–2870. https://doi.org/10.1175/jamc-d-13-073.1
Ryzhkov, A., Snyder, J., Carlin, J., Khain, A., & Pinsky, M. (2020). What polarimetric weather radars offer to cloud modelers: Forward radar operators and microphysical/thermodynamic retrievals. *Atmosphere 2020*, 11, 362. https://doi.org/10.3390/atmos11040362
Ryzhkov, A., Zhang, P., Reeves, H., Kumjian, M., Tschallener, T., Simmer, C., & Troemel, S. (2016). Quasi-vertical profiles—A new way to look at polarimetric radar data. *Journal of Atmospheric and Oceanic Technology*, *33*, 551–562. https://doi.org/10.1175/jtech-d-15-0020.1
Ryzhkov, A., & Zrnić, D. (2019). *Radar Polarimetry for Weather Observations*. Springer, 486 pp.
Ryzhkov, A., Zrnic, D. & Gordon, B. (1998). Polarimetric method for ice water content determination. *Journal of Applied Meteorology*, *37*, 125–134. https://doi.org/10.1175/1520-0450(1998)037<0125:pmfiwc>2.0.co;2
Stanford, M., Varble, A., Zipser, E., Strapp, J., Leroy, D., Schwarzenboeck, A., et al. (2017). A ubiquitous ice size bias in simulations of tropical deep convection. *Atmospheric Chemistry and Physics*, *17*, 9599–9621. https://doi.org/10.5194/acp-17-9599-2017
Stechman, D., McFarquhar, G., Rauber, R., Jewett, B., & Black, R. (2020). Composite in situ microphysical analysis of all spiral vertical profiles executed within BAMEX and PECAN Mesoscale Convective Systems. *Journal of the Atmospheric Sciences*, *77*, 2541–2565. https://doi.org/10.1175/jas-d-19-0317.1
Strapp, J. (2016). *The High Ice Water Content (HIWC) study of deep convective clouds: Science and technical plan (Technical Report, FAA Report DOT/FAA/TC-14/31, p. 105)*. Retrieved from https://www.tc.faa.gov/its/worldpac/techrpt/tc14-31.pdf
Tian, J., Dong, X., Xi, B., Minnis, P., Smith, W., Sun-Mack, S., et al. (2018). Comparison of ice water path in deep convective systems among ground-based, GOES, and CERES-MODIS retrievals. *Journal of Geophysical Research: Atmospheres*, *123*, 1708–1723. https://doi.org/10.1002/2017jd027498

Tian, J., Dong, X., Xi, B., Wang, J., Homeyer, C., McFarquhar, G., & Fan, J. (2016). Retrievals of ice cloud microphysical properties of deep convective systems using radar measurements. *Journal of Geophysical Research: Atmospheres*, *121*, 10820–10839. https://doi.org/10.1002/2015jd024686

Tobin, D., & Kumjian, M. (2017). Polarimetric radar and surface-based precipitation-type observations of ice pellet to freezing rain transitions. *Weather and Forecasting*, *32*, 2065–2082. https://doi.org/10.1175/waf-d-17-0054.1

Troemel, S., Ryzhkov, A., Hickman, B., Muhlbauer, K., & Simmer, C. (2019). Polarimetric radar variables in the layers of melting and dendritic growth at X band—Implications for a nowcasting strategy in stratiform rain. *Journal of Applied Meteorology and Climatology*, *58*, 2497–2522. https://doi.org/10.1175/JAMC-D-19-0056.1

Vivekanandan, J., Bringi, V., Hagen, M., & Meischner, P. (1994). Polarimetric radar studies of atmospheric ice particles. *IEEE Transactions on Geoscience and Remote Sensing*, *32*, 1–10. https://doi.org/10.1109/36.285183

Wu, D., Zhang, F., Chen, X., Ryzhkov, A., Zhao, K., Kumjian, M., et al. (2021). Evaluation of microphysics schemes in tropical cyclones using polarimetric radar observations: Convective precipitation in an outer rain band. *Monthly Weather Review*, *149*, 1055–1068. https://doi.org/10.1175/MWR-D-19-0378.1

Zhang, G. (2016). *Weather radar polarimetry* (p. 322). CRC Press.

Zhang, G., Vivekanandan, J., & Brandes, E. (2001). A method for estimating rain rate and drop size distribution from polarimetric radar measurements. *IEEE Transactions on Geoscience and Remote Sensing*, *39*, 830–841. https://doi.org/10.1109/36.917906

Zhang, J., Tang, L., Cocks, S., Zhang, P., Ryzhkov, A., Howard, K., et al. (2020). A dual-polarization radar synthetic QPE for operations. *Journal of Hydrometeorology*, *21*, 2507 – 2521, https://doi.org/10.1175/JHM-D-19-0194.1